SEMI-LAGRANGIAN EXPONENTIAL INTEGRATION WITH APPLICATION TO THE ROTATING SHALLOW WATER EQUATIONS *

PEDRO S. PEIXOTO† AND MARTIN SCHREIBER‡

Abstract. In this paper we propose a novel way to integrate time-evolving partial differential equations that contain nonlinear advection and stiff linear operators, combining exponential integration techniques and semi-Lagrangian methods.

The general formulation is built from the solution of an integration factor problem with respect to the problem written with a material derivative so that the exponential integration scheme naturally incorporates the nonlinear advection. Semi-Lagrangian techniques are used to treat the dependence of the exponential integrator on the flow trajectories. The formulation is general, as many exponential integration techniques could be combined with different semi-Lagrangian methods. This formulation allows an accurate solution of the linear stiff operator, a property inherited by the exponential integration technique. It also provides an accurate representation of the nonlinear advection, even with large time step sizes, a property inherited by the semi-Lagrangian method.

Aiming for application in weather and climate modelling, we discuss possible combinations of well established exponential integration techniques and state-of-the-art semi-Lagrangian methods used operationally in the application. We show experiments for the planar rotating shallow water equations revealing that traditional exponential integration techniques could benefit from this formulation with semi-Lagrangian to ensure stable integration with larger time step sizes. From the application perspective, which already uses semi-Lagrangian methods, the exponential treatment could improve the solution of wave-dispersion when compared to semi-implicit schemes.

Key words. Exponential integrator, semi-Lagrangian, nonlinear advection, rotating shallow water equations, weather and climate modelling.

AMS subject classifications. 65M99, 65N99, 76B60, 76U05

1. Introduction.

Consider an autonomous initial value problem of the form

$$\frac{du}{dt} = \mathcal{L}(u) + \mathcal{N}(u), \quad u(0) = u_0 \tag{1}$$

where $\mathcal{L}$ is a linear (possibly differential) operator and $\mathcal{N}$ is a function (usually nonlinear). The linear operator $\mathcal{L}$ may come from the original problem or be defined from a linearization of a more general autonomous system. Exponential integrators are usually derived making use of exponentials of a discrete form of the linear operator $\mathcal{L}$. Many schemes of this form exists, as one may notice from the review of [27].

Several application models, such as those related to fluid dynamics [1], have an important advection term in the equations, usually nonlinear. This can be represented as

$$\frac{Du}{Dt} = \frac{\partial u}{\partial t} + \vec{v} \cdot \nabla u = \mathcal{L}(u) + \tilde{\mathcal{N}}(u), \quad u(0) = u_0, \tag{2}$$

where D/Dt represents a total or material derivative, $\vec{v} = \vec{v}(t, \vec{x}, u)$ is the advection velocity, $u = u(t, \vec{x})$, $\tilde{\mathcal{N}}$ represents a general nonlinear term and the gradient (∇) acts only on the spatial variables ($\nabla = (\partial_{x_1}, \partial_{x_2}, ..., \partial_{x_n})$).

*Submitted to the editors DATE.

Funding: This work was funded by FAPESP grant 2014/10501-0 and 2016/18445-7, USP-Santander Mobility grant 527/2016 and NCAR funding

†Instituto de Matemática e Estatística, Universidade de São Paulo, Brazil (pedrosp@ime.usp.br, http://www.ime.usp.br/~pedrosp).

‡College of Engineering, Mathematics and Physical Sciences, University of Exeter, UK (M.Schreiber@exeter.ac.uk, http://www.martin-schreiber.info).

The treatment of the nonlinear advection in exponential integrators varies and leads to different mathematical properties. It can, for instance, be simply thought as a nonlinear term in the exponential integration scheme [7]. Also, the nonlinear term can be treated via a linearization procedure [13, 34, 8, 52, 22, 30], which can depend on the computation of Jacobian matrices or not.

A well-established method to solve equations with nonlinear advection is the semi-Lagrangian advection approach [47, 41, 55, 17]. The cost-effectiveness of semi-Lagrangian schemes depends on the problem [5]. They are used in computational fluid dynamics [60, 11], and are very successfully used in weather forecasting [58], hence being adopted by several weather forecasting centres in operational models [15, 4, 20, 38]. Semi-Lagrangian schemes preserve a fixed grid but follow particle trajectories for each time step to obtain precise information about the advected quantities. These schemes usually have very low dispersion errors [46], but are computationally more expensive than, for example, usual finite difference schemes for one single time step. However, when coupled with an implicit treatment of fast linear waves, this kind of scheme usually allows time step sizes that compensates the additional computational effort, with a reduced wall-clock time.

Exponential integrators and semi-Lagrangian schemes have an interesting connection. For linear advection, the characteristics (which define a particle trajectory) are precisely given by the exponential of the linear advection operator [9]. Moreover, for nonlinear advection, it is possible to establish an equivalence between the solution of a general integration factor problem to a semi-Lagrangian approach [54]. Therefore, it is possible to obtain properties of semi-Lagrangian schemes considering them from an exponential operator point of view. Or, similarly, it is possible to consider the solution of a semi-Lagrangian problem in place of an operator exponential [10]. The latter allows, for example, the development of high order semi-Lagrangian schemes [11].

The goal of this work is to explore a combination of both approaches: semi-Lagrangian and exponential integrators. The key development in this paper is to consider an exponential integration scheme that is built with respect to the total (material) derivative, therefore treats nonlinear advection within the exponentiation framework, which, to our knowledge, has not yet been explored in the literature. With this methodology, nonlinear advection is calculated accurately with low dispersion error (property earned from the semi-Lagrangian approach), in combination with an accurate solution of the linear problem even for very stiff hyperbolic problems (property earned from the exponential integration). In principle, several combinations of exponential integration and semi-Lagrangian schemes could be explored. We will derive the general principles of the method and then illustrate how well-established schemes can be used together.

The main application envisioned is modelling geophysical fluid dynamics, with implications in weather forecasting and climate modelling, where semi-Lagrangian schemes are already used operationally [15, 4, 20, 38]. Such applications are experiencing a recent computational bottleneck, as traditional schemes are reaching the limits of horizontal scalability [58]. This is particularly problematic for climate and paleoclimate simulations, that use a relatively low resolution and long-time integration ranges, which would lead to wall-clock times of several months. In this scenario, there is a renewed interest in novel time stepping schemes that allow larger time steps, preserving accuracy, as well as better exploiting machine parallelism, targeting reduced wall-clock time. Also, traditional geophysical fluid dynamics models usually employ either an explicit time stepping scheme, for which the time step sizes are constrained by faster waves in the system (e.g inertia-gravity), or implicit time stepping schemes (e.g. Crank-Nicolson), which allow larger time steps, at the cost of damping the faster (short wavelength) linear waves. For atmospheric dynamics, such implicit schemes usually damp the faster gravity waves. A recent review on the matter of time stepping schemes for weather and climate [38] points out the need of time integration schemes that allow large time steps while preserving wave dispersion properties. Small scale horizontal gravity waves play an important role in the large structure of the middle atmosphere, particularly for climate simulations [37]. Exponential integrators provide a way to obtain large time steps without damping these small-scale waves, preserving superior linear dispersion properties. However, exponential integrators can be usually more expensive than traditional implicit schemes, but this cost may be compensated by additional degrees of parallelism and larger time step sizes [51].

An important model for the atmosphere and ocean dynamics is formed by the two-dimensional nonlinear rotating shallow water equations (SWE), as they provide a simple set of equations that already carry many of the complications encountered in full three-dimensional dynamics. Recent works of [13] and [23] explored the use of exponential integrators in SWE and showed its potential and practical relevance to weather forecasting. They explored the dynamic linearization procedure of [56] to obtain their exponential integrator, and the nonlinear advection was treated within the linearization. Also within this application framework, [22] shows results from exponential integrator schemes for Boussinesq thermal convection, indicating higher computational cost but greater accuracy with respect to well established schemes for the problem. Considering linear equation sets for this application, [3] solves the linear advection problem on the sphere, which is an important test case for weather and climate, using exponential integration. Also, [51] solves the linear SWE with a rational exponential integrator and analyze the potential computational gain of their massively parallel scheme. However, the practical adequacy of exponential integration schemes for weather and climate is still a matter of research, for which this study hopes to contribute.

A combination with similarities to the one proposed here was developed by [12] where, instead of deriving the exponential integration along trajectories, a Laplace transform following trajectories was used. They also analyze how this semi-Lagrangian Laplace transform method can improve certain aspects of the solutions obtained with traditional semi-Lagrangian semi-implicit scheme considering a shallow water model. They particularly show how the Laplace transform method allows a filtering of an issue encountered in the semi-implicit scheme, known as orographic resonance. Such filtering could also be developed along similar lines for the semi-Lagrangian exponential schemes derived here.

The paper is organised as follows. In Section 2 we review usual exponential integration techniques. In Section 3 we review usual semi-Lagrangian techniques. These two sections will be used in the development of the semi-Lagrangian exponential technique, which is shown in Section 4. Section 5 shows properties of the SWE, which be investigated numerically in Section 6. We finish the paper with some remarks in Section 7.

2. Exponential integration.

We start providing a brief review of some existing exponential integration techniques that will be relevant for the semi-Lagrangian exponential approach. More details may be found in the review of exponential integrators of [27] and in references therein.

2.1. Analytical time integration. Numerically, the solution of equation (1), $u(t)$, is approximated by (n) discrete values that could be, for example, grid point values or spectral coefficients, or both. This defines the discrete solution $U(t) \in \mathbb{R}^n$ evolving in time. The linear operator $(\mathcal{L})$ can be approximated by a discrete version of it (L), with a preferred discretization scheme. Since L may be originated from a partial differential equation problem, it is prudent to keep in mind that L may be a function of the spatial coordinates (or wavenumbers). However, having derived it for an autonomous system, it is independent of time. So the analogous semi-discrete problem of interest may be written as

$$\frac{dU(t)}{dt} = LU(t) + N(U(t)), \quad U(0) = U_0, \tag{3}$$

where $L \in \mathbb{R}^n \times \mathbb{R}^n$ is the discrete linear operator (an $n \times n$ matrix) and $N(U)$ is a discrete version of $\mathcal{N}(u)$.

Now let's assume that $U(t_n)$ is given for a current time t_n, and that we wish to calculate $U(t_{n+1})$, for $t_{n+1} = t_n + \Delta t$. Since L may depend only on spatial variables, but not time, the integration factor problem,

$$\frac{dQ_n(t)}{dt} = -Q_n(t)L, \quad Q_n(t_n) = I, \tag{4}$$

where I is the identity matrix, has a unique solution given by

$$Q_n(t) = e^{-(t-t_n)L}. \tag{5}$$

Using the integration factor in equation (3) one sees that

$$\frac{d}{dt}\left(Q_n(t)U(t)\right) = Q_n(t)N(U). \tag{6}$$

Therefore the problem has an exact solution which may be implicitly represented as,

$$U(t_{n+1}) = Q_n^{-1}(t_{n+1})U_0 + Q_n^{-1}(t_{n+1}) \int_{t_n}^{t_{n+1}} Q_n(s)N(U(s))ds, \tag{7}$$

where we note that $Q_n^{-1}(t) = e^{(t-t_n)L}$ is the inverse of $Q_n(t)$, and thus

$$U(t_{n+1}) = e^{\Delta t L}U(t_n) + e^{\Delta t L} \int_{t_n}^{t_{n+1}} e^{-(s-t_n)L} N(U(s))ds, \tag{8}$$

which is well-known as the variation-of-constants formula.

2.2. Numerical time integration (ETDRK). Exponential integration makes use of calculations of the exponentials, and/or exponential related functions, to obtain a time marching scheme along the lines of equation (8). There are many ways to obtain efficient calculations of matrix exponentials, as may be seen in [39]. We will postpone the discussion about how we intend to calculate the matrix exponential to a further section. For now, we simply assume that a precise method to obtain the exponential is known.

The key differences in exponential integrator schemes lays in the way the nonlinear term is evaluated. If the equation is purely linear ($N = 0$), then the integral term in equation (8) vanishes and it is possible to solve the problem directly from the matrix exponential calculation for each time step. For nonlinear problems, there exists several approaches [27]. We will use as example the Runge-Kutta Exponential Time Differencing (ETDRK) methods, following [14]. However, for the semi-Lagrangian exponential scheme (to be shown), other methods could be considered in a similar fashion.

As a first order approximation, let the nonlinear term $N(U)$ in the integral be constant in time, for each time step, with value $N(U(t_n))$. We can then formally derive what is known as the first order ETD1RK method. Using equation (4) and assuming L^{-1} exists, we may formally write

$$\begin{aligned}
U(t_{n+1}) &= e^{\Delta t L}U(t_n) + \left(\int_{t_n}^{t_{n+1}} e^{-(s-t_{n+1})L} ds\right) N(U(t_n)) + \mathcal{O}(\Delta t) \\
&= e^{\Delta t L}U(t_n) - \left(\int_{t_n}^{t_{n+1}} L^{-1}\frac{d\left(e^{-(s-t_{n+1})L}\right)}{ds} ds\right) N(U(t_n)) + \mathcal{O}(\Delta t) \\
&= e^{\Delta t L}U(t_n) + L^{-1}\left(e^{\Delta t L} - I\right) N(U(t_n)) + \mathcal{O}(\Delta t), \qquad (9) \\
&= \varphi_0(\Delta t L)U(t_n) + \Delta t\, \varphi_1(\Delta t L) N(U(t_n)) + \mathcal{O}(\Delta t),
\end{aligned}$$

where,

$$\varphi_0(z) = e^z, \qquad \varphi_1(z) = z^{-1}(e^z - 1) \qquad (10)$$

with $z = \Delta t L$.

In many problems L^{-1} is not well defined, since, for example, L may have null eigenvalues. However, under the assumption that L is a finite dimensional matrix, φ_1 is always well defined if the pseudo-inverse is considered (note that in case L has null eigenvalues the nominator also leads to null values).

More general (higher order) ETD schemes may be derived using higher order φ_k functions (see [14]), which may be defined as

$$\varphi_k(z) = z^{-k}(e^z - t_{k-1}(z)), \quad t_k = \sum_{l=0}^{k} \frac{z^l}{l!} \qquad (11)$$

or using the recurrence relation

$$\varphi_{k+1}(z) = z^{-1}\left(\varphi_k(z) - \varphi_k(0)\right), \quad \varphi_0(z) = e^z, \qquad (12)$$

where potential singularities may be, in the present work, treated noticing that in the limit of $z \to 0$ the l'Hopital rule can be applied.

We will be particularly interested in this paper in the second order ETDRK scheme, in order to allow a fair comparison to other well-established second order approaches in our numerical experiments. Let U^n be the numerical approximation of $U(t_n)$ at time t, then the ETD2RK scheme may be written as

$$\begin{aligned}
U_1^{n+1} &= \varphi_0(\Delta t L)U^n + \Delta t\, \varphi_1(\Delta t L) N(U^n), \\
U^{n+1} &= U_1^{n+1} + \Delta t \varphi_2(\Delta t L)\left(N(U_1^{n+1}) - N(U^n)\right), \qquad (13)
\end{aligned}$$

which is derived substituting the second order approximation for the nonlinear term,

$$N(U(s)) = N(U(t_n)) + \frac{(s-t_n)}{\Delta t}\left(N(U_1(t_{n+1})) - N(U(t_n))\right) + \mathcal{O}(\Delta t^2), \qquad (14)$$

into equation (8).

3. Semi-Lagrangian integration.

Broadly, Lagrangian schemes usually follow particle trajectories (characteristics) through time and may not even rely on a fixed computational grid, or else have a grid evolving over time. This can create complicated grids structures involving, for example, intersections of trajectories. Eulerian schemes usually keep a fixed grid and evaluate the movement of the particles that pass through a computational cell. For nonlinear advection, these schemes usually have time step size limited by the Courant-Friedrichs-Lewy condition (CFL). Semi-Lagrangian schemes keep a fixed grid but follow the particle trajectories for a single time step (a local version of the classical Lagrangian approach). Since the trajectories may end, or start, in points not in the reference grid, usually an interpolation step is required. In the context of atmospheric simulations, the scheme usually allows time step sizes larger than Eulerian schemes, beyond CFL condition [48], and reduces the risk intersecting trajectories with respect to fully Lagrangian schemes.

In this section we introduce classic notations and results about semi-Lagrangian schemes. This will be required as a basis to derive the semi-Lagrangian exponential schemes in the next section. Further details on semi-Lagrangian methods can be found in [55] and [17].

3.1. The material derivative.

We start considering Equation (2) on a Lagrangian framework, relative to a particle initially positioned at $\vec{r}_0$ in space. Thus, the system state is formed by $u = u(t, \vec{r}(t))$, with advection velocity defined as $\vec{v} = \vec{v}(t, \vec{r}(t), u(t, \vec{r}(t)))$. Here, $\vec{r}(t)$ is the Lagrangian trajectory of the particle, therefore it is the solution of the non-autonomous problem

$$\frac{d\vec{r}(t)}{dt} = \vec{v}(t, \vec{r}(t), u(t, \vec{r}(t))), \quad \vec{r}(0) = \vec{r}_0. \tag{15}$$

Equation (2) may be written in a Lagrangian framework as

$$\frac{du(t, \vec{r}(t))}{dt} = \mathcal{L}(u(t, \vec{r}(t))) + \tilde{\mathcal{N}}(u(t, \vec{r}(t))), \quad u(0, \vec{r}_0) = u_0, \tag{16}$$

where now $\mathcal{L}$ and $\tilde{\mathcal{N}}$ may implicitly also depend on the position $\vec{r}(t)$. The time derivative is expanded as

$$\frac{du(t, r(t))}{dt} = \frac{\partial u(t, \vec{r}(t))}{\partial t} + \vec{v} \cdot \nabla u(t, \vec{r}(t)). \tag{17}$$

This time derivative on the Lagrangian framework is usually denoted as a total (material) derivative. To simplify the notation and avoid confusion with equation (1) this derivative is sometimes denoted in capital letters as D/Dt, so that we can simply write, without ambiguity, that equation (16) is

$$\frac{Du}{Dt} = \mathcal{L}(u) + \tilde{\mathcal{N}}(u), \quad u(0) = u_0. \tag{18}$$

As in the previous section, we will focus here on a discretized problem, where $\mathcal{L}$ may be again directly viewed as a finite dimensional matrix operator, hence linear, and will be denoted by L. In a Lagrangian framework, L may depend on the particle position $\vec{r}(t)$. Therefore, we may analogously to equation (3) set the general non-autonomous semi-discrete problem to be

$$\frac{DU(t, \vec{r}(t))}{Dt} = L(U(t, \vec{r}(t))) + \tilde{N}(U(t, \vec{r}(t))), \quad U(t_0, \vec{r}(t_0)) = U^0, \tag{19}$$

where $\tilde{N}$ is a numerical approximation to $\tilde{\mathcal{N}}$, and now the time differential is a total derivative and depends on the solution of the problem given in (15).

Although there are many forms of semi-Lagrangian schemes [55], these usually rely on basically two parts: (i) the evaluation of the trajectories (characteristics), which are solutions of the problem (15), and (ii) the interpolation of the information to the reference grid. Both parts play important roles in the accuracy and stability of the schemes [19, 17, 40]. We will consider a back-trajectory approach, which is a well-established approach [29] that assumes that the grid is fixed at time t_{n+1}. The trajectory determines the position of a departure point at time t_n, which is likely not to be a grid point, so an interpolation of the advected quantity is required. As shown in [19], the interpolation order needs to be chosen in agreement with the accuracy order of the trajectory calculation.

3.2. Trajectory calculations. The trajectory evaluation can be obtained by a direct numerical time integration of differential equation (15), as a sub-cycling procedure, or, which is more common in atmospheric applications, solve its integral form. In the later,

$$\vec{r}(t_{n+1}) - \vec{r}(t_n) = \int_{t_n}^{t_{n+1}} \vec{v}(t, \vec{r}(t), u(t, \vec{r}(t)))dt, \tag{20}$$

is solved to obtain the departure point $\vec{r}_d = \vec{r}(t_n)$ from the knowledge of the arrival point $\vec{r}_a = \vec{r}(t_{n+1})$, which is set to be a grid point.

Simple two-time level schemes [36] can be build using, for example, the midpoint rule integration (for $\vec{r}_m = \vec{r}(t_{n+1/2})$) and an iterative procedure to solve the nonlinear resulting equation.

In case $\vec{v}$ is not known within $[t_n, t_{n+1}]$, for example if $\vec{v}$ depends on u, its evaluation in intermediate times requires an extrapolation from previous time steps. This extrapolation may directly influence the stability of the scheme [17]. A well-established approach is the Stable Extrapolation Two-Time-Level Scheme (SETTLS) of [29], used in the ECMWF[1] in their global spectral model IFS. This method adopts an extrapolation such that the velocity at the midpoints can be approximated with second order as

$$\underbrace{\vec{v}(t_{n+1/2}, \vec{r}_m, u_m)}_{\text{Midpoints}} = \frac{1}{2}\left[\underbrace{2\vec{v}(t_n, \vec{r}_d, u(t_n, \vec{r}_d)) - \vec{v}(t_{n-1}, \vec{r}_d, u(t_{n-1}, \vec{r}_d))}_{\text{Departure points}} + \underbrace{\vec{v}(t_n, \vec{r}_a, u(t_n, \vec{r}_a))}_{\text{Arrival points}}\right]. \tag{21}$$

The fields to be calculated at the departure points, such as $\vec{v}(t_n, \vec{r}_d^{\,k}, u(t_n, \vec{r}_d^{\,k}))$, are obtained by first calculating $\vec{v}(t_n, \vec{x}, u(t_n))$ at the usual grid points, and then interpolating to the departure points $\vec{r}_d^{\,k}$. Consequently, the departure points may be obtained through an iterative procedure with

$$\vec{r}_d^{\,k+1} = \vec{r}_a - \frac{\Delta t}{2}\vec{v}(t_n) - \frac{\Delta t}{2}\left(2\vec{v}(t_n) - \vec{v}(t_{n-1})\right)_*^n. \tag{22}$$

where the subscript $_*$ with superscript ^{n} denotes interpolation to $\vec{r}_d^{\,k}$ points [6]. As first guess, $\vec{r}_d^{\,0} = \vec{r}_a$ is assumed. For smooth flows, a few iterations (3 or 4) are usually sufficient to ensure an accurate solution of the nonlinear equation.

[1] European Centre for Medium-Range Weather Forecasts

3.3. Semi-Lagrangian Solver (SL-SI-SETTLS). A well-established semi-Lagrangian solver for atmospheric models is the scheme used in the IFS-ECMWF model. It uses a semi-Lagrangian scheme coupled with a semi-implicit time stepping of linear terms with spectral horizontal discretization. This scheme, based on [29], will serve as a first guideline in the development of the semi-Lagrangian exponential schemes.

The semi-implicit discretization with semi-Lagrangian Crank-Nicolson time stepping assumes

$$\frac{U^{n+1}-U_*^n}{\Delta t} = \frac{1}{2}\left((LU)^{n+1} + (LU)_*^n\right) + \tilde{N}^{n+1/2}, \tag{23}$$

where the last term represents the non-linearities at the midpoint of the trajectory. This term is computed based on averaging and extrapolation (see [29], Eq. (4.4,4.5)) with

$$\tilde{N}^{n+1/2} = \frac{1}{2}\left(\left[2\tilde{N}^n - \tilde{N}^{n-1}\right]_* + \tilde{N}^n\right), \tag{24}$$

which is the SETTLS extrapolation, where $\tilde{N}_n$ is the evaluation of the nonlinear term at time t_n. The unknowns in Equation (23) are implicitly given by U^{n+1} and $(LU)^{n+1}$, which require a linear solver.

To ensure an overall second order accurate scheme (assuming $\Delta t \propto \Delta x$), it is sufficient to use cubic interpolations of the advected quantities (with respect to Equations (23) and (24)), and linear interpolations of the velocities in the trajectory calculations (Equation (22)) [40].

4. Semi-Lagrangian exponential integration. In this section, we discuss how the general exponential integration techniques can be applied in a Lagrangian reference frame. Exponential integration schemes usually incorporate the nonlinear advection into the nonlinear term calculation or solve about a linearization of it. We propose a new scheme which is described as follows.

4.1. Basic theory. The key concept investigated in this paper is to consider, from a numerical perspective, the exponential integration of Equation (19) considering the total (material) derivative.

As in Section 2, where we built exponential integration schemes from the solution of an integration factor problem, we would like to be able to define a similar integration factor for the problem with respect to this material derivative. We assume the existence of an integration factor $P_n(t)$ that is a solution to the problem

$$\frac{D(P_n(t)\,U(t,\vec{r}(t)))}{Dt} = P_n(t)\tilde{N}(U(t,\vec{r}(t))), \quad P_n(t_n) = I. \tag{25}$$

Assuming that U is solution of (19), P_n will also be a solution of

$$\frac{DP_n(t)}{Dt}U(t,\vec{r}(t)) = -P_n(t)L(U(t,\vec{r}(t))), \quad P_n(t_n) = I. \tag{26}$$

We recall that L may depend on the space variables, which are now dependent also on time due to the Lagrangian framework, which we will explicitly indicate with a subscript as $L = L_{\vec{r}(t)}$. If $L_{\vec{r}(t)}$ commutes in time, that is, $L_{\vec{r}(t)}L_{\vec{r}(s)} = L_{\vec{r}(s)}L_{\vec{r}(t)}$ for all times s and t, then the integration factor problem has as solution

$$P_n(t) = e^{-\int_{t_n}^{t} L_{\vec{r}(s)}ds}. \tag{27}$$

For the continuous problem with L with space-varying coefficients (dependent of the particle position), the commutation assumption will most likely not be satisfied. The integration factor may, however, still exist and be well defined, but might not have the usual matrix exponential form. Assuming that such integration factor exists, and that it is invertible (P_n^{-1} exists for all time), equations (19) and (25) indicate the following implicit relation on U (analogous to (7)),

$$U(t_{n+1},\vec{r}(t_{n+1})) = P_n^{-1}(t_{n+1})U(t_n,\vec{r}(t_n)) + P_n^{-1}(t_{n+1})\int_{t_n}^{t_{n+1}} P_n(s)\tilde{N}(U(s,\vec{r}(s)))ds. \tag{28}$$

This is the fundamental equation for the derivation of the semi-Lagrangian exponential schemes developed in this paper.

Numerically, one needs an explicit way of calculating the integration factor. This will depend on the problem of interest. One possibility is to directly numerically integrate equation (26), which is the basis of many operator splitting techniques [54].

Another possibility, if such integration factor is unknown in its exponential form, is to assume that L does not vary within each time step for each given local trajectory, since then the problem reduces to a matrix exponential problem. This should provide a first order approximation to the true integration factor at each time step, but the consequences of this choice for the proposed semi-Lagrangian exponential scheme in terms of overall convergence of the numerical scheme to the solution of the continuous problem is a matter still to be investigated, and will not be further addressed in this paper. Instead, we will assume in what follows that L is independent of the particle position for each time step. This greatly simplifies the problem, as in this case $P_n = Q_n$, as defined in equation (5), and the problem reduces to

$$U(t_{n+1},\vec{r}(t_{n+1})) = e^{\Delta t L}U(t_n,\vec{r}(t_n)) + e^{\Delta t L}\int_{t_n}^{t_{n+1}} e^{-(s-t_n)L}\tilde{N}(U(s,\vec{r}(s)))ds. \tag{29}$$

This is almost identical to what we obtained for the usual exponential integration approach (see equation (8)), but now U is varying along a particle trajectory in time, resulting in a derivation of what we are calling a semi-Lagrangian exponential integration.

Using the semi-Lagrangian notation, we rewrite the numerical method from equation (29) as

$$U^{n+1} = e^{\Delta t L}U_*^n + e^{\Delta t L}\int_{t_n}^{t_{n+1}} e^{-(s-t_n)L}\tilde{N}(U(s,\vec{r}(s)))ds, \tag{30}$$

where U^{n+1} is given at grid points and U_*^n refers to the (interpolated) value at departure points. Therefore, different semi-Lagrangian exponential schemes can be built depending on how the integral is approximated, as happens with the usual exponential integration techniques.

We now highlight two important remarks:

(R1) The semi-Lagrangian schemes are built considering interpolations at non grid points (departure points). The integral in (30) relies on a linear operator (the exponential of L) acting on a nonlinear function ($\tilde{N}$). If we wish to evaluate this at time t_n, therefore at departure points, we should first apply the linear operator to the nonlinear function at time t_n, and only then interpolate to the departure points. If we first interpolate the nonlinear function to the departure points, then the application of the linear operator would be referring to an irregular grid, therefore possibly not being well defined numerically. Therefore, at time t_n, the interpolation should preferably come after the application of the linear operators.

(R2) At time t_{n+1}, interpolated values considering a semi-Lagrangian approach are assumed to have already been advected, therefore the results lay on a regular grid relative to the arrival points, for example as in the U_*^n term of Equation (30). Therefore, at time t_{n+1}, the operators can come after the interpolation.

The main reasons behind these important remarks above are related to the following properties of linear operators acting on advected quantities. Even thought $e^{\Delta t L}$ is a linear operator independent of time and space, it does not in general commute with the interpolation operator ($_*$), since this interpolation reflects a non-regular grid formed by nonlinear back trajectories. Therefore, in general, $e^{\Delta t L} U_*^n \neq \left(e^{\Delta t L} U^n\right)_*$. We provide in Appendix A an illustration for this issue, which happens even in the case of linear advection.

4.2. Semi-Lagrangian Exponential SETTLS (SL-EXP-SETTLS). Following the SETTLS scheme [29] for the semi-Lagrangian discretization, but using it with respect to equation (30), we may derive our first combination of semi-Lagrangian exponential scheme, which we will denote as SL-EXP-SETTLS. The scheme is derived from (30) as

$$U^{n+1} = e^{\Delta t L} U_*^n + \Delta t\, e^{\Delta t L} \tilde{N}_e^{n+1/2}, \tag{31}$$

where we use the SETTLS extrapolation to obtain the value of $\tilde{N}$ at the trajectory midpoint as

$$\tilde{N}_e^{n+1/2} = \frac{1}{2}\left[2\tilde{N}^n - e^{\Delta t L}\tilde{N}^{n-1}\right]_*^n + \frac{1}{2}\tilde{N}^n. \tag{32}$$

To save evaluations of the exponential terms, which are the computationally most intensive parts, one may simplify the above equations in order to require only 2 exponential evaluations per time step.

This scheme may also be thought as a semi-Lagrangian version of the Integrating Factor method, proposed in [14], as the second order Adams-Bashforth Integrating Factor method (IFAB2), as one can notice from their equation (31). Therefore this scheme may also be termed as SL-IFAB2.

As discussed in [14], the concept of stability for Integrating Factor methods is unclear. This is also the case for our semi-Lagrangian version of exponential schemes, and therefore this is a topic discussed purely from a numerical perspective in this paper, with theoretical analysis to be addressed in a later publication.

An illustration of the importance of remark (R1) from the previous sub-section can be shown in the following example. One might think of using a half-time step exponential to incorporate the nonlinearities, deriving the following scheme:

$$U^{n+1} = e^{\Delta t L} U_*^n + \Delta t\, e^{\frac{\Delta t}{2} L} \tilde{N}_a^{n+1/2}, \quad \text{(unstable example)} \tag{33}$$

$$\tilde{N}_a^{n+1/2} = \frac{1}{2}\left[2\tilde{N}^n - \tilde{N}^{n-1}\right]_* + \frac{1}{2}\tilde{N}^n, \tag{34}$$

which applies the extrapolation only on $\tilde{N}$, and will numerically differ from the approach derived above. However, this alternative scheme turns out to be critically unstable, as the extrapolation needs to be applied with respect to the full integrand term.

4.3. Semi-Lagrangian Exponential ETDRK (SL-ETDRK). To construct semi-Lagrangian Exponential Time Differencing Runge-Kutta schemes (SL-ETDRK) in analogy to usual ETDRK schemes, we need to pay attention to the remarks (R1) and (R2) above. In usual ETD schemes, as shown in section 2, the exponential in from of the integral in equation (30) would be commuted with the integral to within the integrand. However, since now the integral is along trajectories, this no longer results in an equivalent problem in the numerical scheme, due the remarks pointed out above. Therefore, we should first evaluate the integral term, and then apply the linear operator ($e^{\Delta t L}$).

To be able to preserve $e^{\Delta t L}$ outside of the integral, and still make use of the φ functions of ETDRK schemes, we may use the following property of φ functions. The $\varphi_0(z) = e^z$ function can be factored out of $\varphi_k(z) = \varphi_0(z)\psi_k(z)$ with

$$\psi_k(z) = (-1)^{n+1}\varphi_k(-z) + \sum_{l=1}^{k-1} \varphi_l(-z). \tag{35}$$

This formula can be proved substituting equation (11) into the right-hand-side of the equation above and using binomial expansions in a similar way as done in [14].

With this property in hand, we may derive the semi-Lagrangian ETD1RK scheme in the following way. From equation (29), assuming as in ETD1RK that the non-linearity is constant within a time step, we have

$$U_1(t_{n+1}, \vec{r}(t_{n+1})) = \varphi_0(\Delta t L)U(t_n, \vec{r}(t_n)) + \varphi_0(\Delta t L)\left(\int_{t_n}^{t_{n+1}} e^{-(s-t_n)L}\right) N(U(t_n, \vec{r}(t_n)))ds. \tag{36}$$

Using the properties of φ functions, particularly that $\varphi_1(z) = \varphi_0(z)\varphi_1(-z)$, we may write the numerical scheme as

$$U_1^{n+1} = \varphi_0(\Delta t L)\left[U^n + \Delta t\, \varphi_1(-\Delta t L) N(U^n)\right]_*^n, \tag{37}$$

which can be computed numerically with only two φ function evaluations and one interpolation per time step.

Deriving the second order scheme (SL-ETD2RK) involves a more careful analysis of how the integral in equation (29) is approximated. Let

$$N(U(s)) = N(U(t_n, \vec{r}(t_n))) + \frac{(s-t_n)}{\Delta t}\left(N(U_1(t_{n+1}, \vec{r}(t_{n+1}))) - N(U(t_n, \vec{r}(t_n)))\right) + \mathcal{O}(\Delta t^2), \tag{38}$$

then

$$\begin{aligned}
U_2(t_{n+1}, \vec{r}(t_{n+1})) &= \varphi_0(\Delta t L)U(t_n, \vec{r}(t_n)) + \varphi_0(\Delta t L)\left(\int_{t_n}^{t_{n+1}} e^{-(s-t_n)L}\right) N(U(t_n, \vec{r}(t_n)))ds \\
&+ \varphi_0(\Delta t L)\left(\int_{t_n}^{t_{n+1}} \frac{(s-t_n)}{\Delta t} e^{-(s-t_n)L}\right) N(U(t_{n+1}, \vec{r}(t_{n+1})))ds \\
&- \varphi_0(\Delta t L)\left(\int_{t_n}^{t_{n+1}} \frac{(s-t_n)}{\Delta t} e^{-(s-t_n)L}\right) N(U(t_n, \vec{r}(t_n)))ds.
\end{aligned} \tag{39}$$

Using the SL-ETD1RK scheme and the properties of the φ functions we may write the SL-ETD2RK scheme as

$$U_2^{n+1} = U_1^{n+1} + \Delta t\, \varphi_0(\Delta t L)\left[\psi_2(\Delta t L)N(U_1^{n+1}) - \left(\psi_2(\Delta t L)N(U^n)\right)_*^n\right], \tag{40}$$

where

$$\psi_2(\Delta t L) = -\varphi_2(-\Delta t L) + \varphi_1(-\Delta t L). \tag{41}$$

The cost of a ψ function evaluation is similar to the cost of a φ function evaluation, as the multiple φs to be summed may be joined in the solver. Therefore, after suitably rearranging the equations, the scheme can be coded to require 4 φ (or ψ) function evaluations and 2 interpolations.

5. Rotating Shallow Water Equations on an f-Plane. In this section we describe the basic concepts of the Shallow Water Equations (SWE), which will serve as application for the schemes discussed in the previous sections.

Considering a Lagrangian framework, with particle trajectories given by $\vec{r}(t) = (x(t), y(t))$ on a plane, we define $\vec{v} = \vec{v}(t, \vec{r}(t)) = (u(t, \vec{r}(t)), v(t, \vec{r}(t)))$ to be the flow velocity, and $\eta = \eta(t, \vec{r}(t))$ a fluid depth perturbation about a constant mean fluid depth ($\bar{\eta}$). The rotating SWE on an f-plane may then be written as

$$\frac{DU}{Dt} = \mathcal{L}U + \tilde{\mathcal{N}}(U), \tag{42}$$

where the time derivative is assumed to be the total (material) derivative, and

$$U = \begin{pmatrix} u \\ v \\ \eta \end{pmatrix}, \quad \mathcal{L} = \begin{pmatrix} 0 & f & -g\partial_x \\ -f & 0 & -g\partial_y \\ -\bar{\eta}\partial_x & -\bar{\eta}\partial_y & 0 \end{pmatrix}, \quad \tilde{\mathcal{N}}(U) = \begin{pmatrix} 0 \\ 0 \\ -\eta\nabla\cdot\vec{v} \end{pmatrix}, \tag{43}$$

where the total fluid depth h is given by $h = \eta + \bar{\eta}$. The velocities are given by $\vec{v} = (u, v)$ and the gravity g is assumed constant. The Coriolis parameter f is assumed to be constant throughout this paper (f-plane approximation). Initial conditions for the prognostic variables (u, v, η) are assumed to be given. Bi-periodic boundary conditions will be adopted for (x, y) on a rectangular limited set of $\mathbb{R}^2$.

The dynamics of the SWE depend on parameter choices $(f, g, \bar{\eta})$ and on the initial conditions. The gravity wave speed is given by $c = \sqrt{g\bar{\eta}}$. To be physically relevant, the shallow water assumption requires the mean depth ($\bar{\eta}$) to be much smaller than the domain size. The typical barotropic atmospheric dynamics considers relatively large values of $\bar{\eta}$, so that $c \gg u_0$, where u_0 represents a reference wind velocity. In this case, the linear waves are much faster than the nonlinear advection. However, in 3D atmospheric models, or multilayer shallow water models, with many vertical levels, the mean depth ($\bar{\eta}$) is related to what is known in atmosphere and ocean models as an equivalent depth[57], which is inversely proportional to vertical resolution. Therefore, $\bar{\eta}$ is considerably smaller in 3D models, resulting in the possibility of $c \approx u_0$. In this case, nonlinear advection discretization plays an important role and is where semi-Lagrangian exponential schemes may show significant gains in time step size. A complete discussion on derivation and properties of the SWE can be found in basic atmospheric dynamics books (e.g. [57, 28, 35]).

The SWE are used as an intermediate step towards the solution of the full three-dimensional equation set for the dynamics of the atmosphere. well-established models adopt semi-implicit schemes [17, 48], with implicit treatment of linear terms and explicit treatment of nonlinearities. Among the implicit schemes for the linear waves, Crank-Nicolson (trapezoidal differencing) is frequently adopted, as done for example in the IFS model of the ECMWF [18, 29], coupled with a semi-Lagrangian approach.

Modern models that use non-regular spherical grids, such as MPAS [53] or DYNAMICO [16], adopt explicit time stepping procedures based on Runge-Kutta time integration. See [38] for an extensive list and description of the main time stepping schemes used for weather and climate models.

5.1. Exponential of the linear operator. We seek to find the exponential of the linear operator $\mathcal{L}$ where we assume the time step size Δt incorporated into $\mathcal{L}$ by simple scaling. Assuming a double Fourier expansion of U in space on a $[0;2\pi)^2$ periodic domain, we can look at a single mode (single wavenumber) to understand the action of $\mathcal{L}$ in terms of its exponentials. For a fixed time, let U be of the form

$$U_{\vec{k}}(\vec{x}) = e^{i\vec{k}\cdot\vec{x}}\hat{U}_{\vec{k}}, \tag{44}$$

with $\vec{k} = (k_1, k_2)$, $\vec{x} = (x_1, x_2) = (x, y)$, $\hat{U}_{\vec{k}}$ independent of $\vec{x}$ and $i = \sqrt{-1}$. Then

$$\mathcal{L}U_{\vec{k}} = \begin{pmatrix} 0 & f & -gik_1 \\ -f & 0 & -gik_2 \\ -\bar{\eta}ik_1 & -\bar{\eta}ik_2 & 0 \end{pmatrix} \hat{U}_{\vec{k}}, \tag{45}$$

where the matrix above is the matrix symbol of $\mathcal{L}$ (usually denoted as $\mathcal{L}(i\vec{k})$), which has purely imaginary eigenvalues (more details can be found in [35]). The eigenvalues are given by

$$\omega_f(\vec{k}) = 0, \quad \omega_g(\vec{k}) = \pm i\sqrt{f^2 + g\,\bar{\eta}\,\vec{k}\cdot\vec{k}}, \tag{46}$$

where $\omega_f(\vec{k})$ is the steady geostrophic, or vortical, mode and ω_g defines the 2 inertia-gravity wave modes $(\omega_g^-(\vec{k}), \omega_g^+(\vec{k}))$. The eigenvectors can be directly computed from $\mathcal{L}(i\vec{k})$, which we will denote as $\vec{\boldsymbol{\omega}}_f(\vec{k})$, $\vec{\boldsymbol{\omega}}_g^-(\vec{k})$, $\vec{\boldsymbol{\omega}}_g^+(\vec{k})$, according to their respective eigenvalues. Defining $Q = [\vec{\boldsymbol{\omega}}_f(\vec{k}),\ \vec{\boldsymbol{\omega}}_g^-(\vec{k}),\ \vec{\boldsymbol{\omega}}_g^+(\vec{k})]$ as the eigenvector matrix, $\Lambda = [\omega_f(\vec{k}), \omega_g^-(\vec{k}), \omega_g^+(\vec{k})]$ as the diagonal eigenvalue matrix, and using $\mathcal{L}(i\vec{k}) = Q\Lambda Q^{-1}$, the exponential of $\mathcal{L}$ can be directly calculated for the shallow water system through its symbol as

$$e^{\mathcal{L}(i\vec{k})} = Qe^{\Lambda}Q^{-1}, \tag{47}$$

where the e^{Λ} is the diagonal matrix with entries given by the exponential of the respective eigenvalues.

For the studies conducted in the present work we exploit features from double Fourier spectral spatial discretization. This allows us to compute the numerical matrix exponential directly from equation (47). Using this approach will provide an exponential (φ_0) of the linear operator accurate to machine precision. To evaluate $\varphi_n(\Delta t L)$ functions (see Eq. (12)), it is straightforward to verify that we can write

$$\varphi_n(\Delta t\,\mathcal{L}(i\vec{k})) = Q\varphi_n(\Delta t\,\Lambda)Q^{-1} \tag{48}$$

hence computing φ_n element-wise for each diagonal element in Λ.

We would like to emphasize that computing the exponential directly as discussed above is only possible because we are exploiting the orthogonal Fourier basis on the bi-periodic domain acting on a constant linear differential operator. In more general settings, such as on the sphere, non-trivial methods, such as matrix exponentiation techniques, need to be employed. Even though many approaches to calculate exponentials exists, see [27], two approaches are currently most commonly researched in this context, Krylov subspace solvers, and rational approximations. Krylov solvers, such as those presented in [26], are used in [13] and [23] for the matrix exponentiation of a dynamic linearization of the shallow water system. Furthermore, [51] adopts a rational approximation based on [25] for the rotating SWE on the plane, which is also used for the sphere in [50] with a global spectral representation. This rational approximation approach calculates the matrix exponentials with a very high degree of parallelism, so the additional computational costs of the calculating such exponential may be absorbed by extra compute nodes to reduce the time-to-solution.

In this study we will use the analytical linear operator exponential described in equation (47), and we will leave the discussion of computational performance of different exponentiation techniques with respect to the semi-Lagrangian exponential method to be presented elsewhere.

5.2. Dispersion analysis. The linear SWE on an f-plane define a hyperbolic system formed by inertia-gravity (Poincaré) and geostrophic (steady) waves. Numerical schemes should be able to represent well these two kinds of waves. We will adopt in this study spectral spatial discretizations of the linear operator (based on Fourier series), therefore errors in the evaluation of the linear operator are negligible (of machine precision) for each wavenumber. However, the temporal discretization may still be a source of error which can be directly investigated.

Let U be written in wave-like solutions for a single horizontal wavenumber ($\vec{k}$), $U(t,\vec{x}) = e^{\omega(\vec{k})t}e^{i\vec{k}\cdot\vec{x}}\hat{U}_{\vec{k}}$, where $\omega(\vec{k})$ is the (time) frequency oscillation relative to a horizontal (spatial) wavemode $\vec{k}$ and $\hat{U}_{\vec{k}}$ now depends on the initial conditions, but not on $\vec{x}$ and t. Substituting U in the linear SWE results in the previously defined dispersion relations ω_f and ω_g from equation (46). We point out that the frequencies are purely imaginary, therefore of pure hyperbolic nature.

For the linear exponential integration schemes, considering that the matrix exponential is calculated within machine precision, these relations are obtained also within the same accuracy. State-of-the-art weather forecasting systems that do not adopt exponential integration schemes, but mostly Runge-Kutta schemes [53] when explicit, or Crank-Nicolson [29] when implicit (see a complete description in [38]). To ensure large time steps, implicit schemes are preferred, but in this case, the dispersion relations described above are not very accurately attained for the smaller wave-modes (faster gravity waves). Durran [17] discusses this in details for 1D SWE, but we will highlight the analytical dispersion relation of the Crank-Nicolson scheme for our two-dimensional system here for the sake of completeness.

The Crank-Nicolson (CN) scheme, considering analytical evaluation of the space linear operator $\mathcal{L}$, may be written as

$$\frac{U^{n+1}-U^n}{\Delta t} = \frac{1}{2}\left(\mathcal{L}U^{n+1}+\mathcal{L}U^n\right), \tag{49}$$

which leads to an implicit linear system. Using the $\mathcal{L}(i\vec{k})$ matrix symbol eigendecomposition and a wave-like solution discrete-in-time, we obtain the amplification factor for one time step as

$$e^{\Delta t\,\tilde{\omega}(\vec{k})} = \frac{1+\frac{\Delta t}{2}\omega(\vec{k})}{1-\frac{\Delta t}{2}\omega(\vec{k})} \tag{50}$$

where $\tilde{\omega}$ is the approximate dispersion relation of the CN scheme and ω denotes the analytical one. Therefore the CN scheme preserves the steady geostrophic modes (for $\tilde{\omega}_f(\vec{k}) = \omega_f(\vec{k}) = 0$). However, the gravity waves will have dispersion of the form

$$\tilde{\omega}_g(\vec{k}) = \omega_g(\vec{k}) + \frac{\Delta t^2}{12}(\omega_g(\vec{k}))^3 + \mathcal{O}(\Delta t^5), \tag{51}$$

which is purely imaginary (the amplitude of the mode is not altered by the scheme), but the phase speed is affected. The odd powers of ω_g indicate that the additional terms (error) will always produce a reduction of the $\tilde{\omega}_g$ frequency, and this reduction will be larger the larger the wavenumber norm $(\vec{k} \cdot \vec{k})$, since it depends on $\omega_g(\vec{k})$. Therefore, the error in the Crank-Nicolson method slows down the faster (larger wavenumber) inertio-gravity waves, which will be slower when larger time step sizes are used.

For finite difference schemes the spatial errors significantly influence the dispersion relations. [45] analyzes the effect of different discretizations on the shallow water waves dispersions. To preserve an adequate representation of the inertio-gravity waves and reduce computational modes arising from spatial discretizations, staggered grids are preferred. These are usually called C-grids in the geoscientific modelling community, and has the depth variable centred in the cell and the velocities given at the edges of cell, normal to the edge [2]. Finite difference schemes are usually coupled with explicit Runge-Kutta (RK) time integration, which is limited by CFL stability conditions, so the time step size is usually much smaller than with implicit schemes. As it uses small time steps, the dispersion errors are then dominated by the spatial discretization erros. For large scales, finite difference schemes on C-grids represent well the inertia-gravity waves, but they also damp the smaller wavelength waves (faster). See [44] for details on the dispersions with respect to difference time and space finite difference schemes. Since many modern atmospheric models that use non-regular grids are using finite-difference/volumes approaches with explicit time integration, we will also consider this approach as reference in our experiments further in the paper.

6. Numerical experiments.

We will consider the following set of schemes to be analyzed:

- RK-FDC: Runge-Kutta second order in time with second order in space energy conserving finite differences discretization on a staggered C-grid due to [49].
- SL-SI-SETTLS: Semi-Lagrangian, semi-implicit (Crank-Nicolson) scheme using spectral discretization adapted from [29] to the plane, described for the planar SWE in Appendix B.
- SL-EXP-SETTLS: Exponential version of SL-SI-SETTLS, as described in Section 4.2.
- ETD2RK: Original ETD2RK scheme, as described in Section 2, with spectral space discretization.
- SL-ETD2RK: Semi-Lagrangian version of ETD2RK, as described in Section 4.3.
- REF: Reference solution. Runge-Kutta forth order in time with small time step and high resolution Eulerian spectral discretization (pseudo-spectral for all nonlinear terms, such as advection).

The schemes are connected in the following way. RK-FDC is a reference explicit scheme well-established for the solution of the SWE of very low cost per time step, but restricted to smaller time steps (CFL condition). SL-SI-SETTLS is the state-of-the-art scheme used in many global atmospheric dynamical cores, which we aim to compare to our semi-Lagrangian exponential schemes (SL-EXP-SETTLS, SL-EXP-ETD2RK). ETD2RK is a well-established exponential integration technique, which we aim to compare to our semi-Lagrangian version, SL-ETD2RK, considering the different treatment of the nonlinear advection.

6.1. Definitions of domain and parameters. The experiments will be executed on a scenario that mimics the Earth's dimensions, and we will follow the standard spherical test case parameters defined in [59]. The domain is set to be $[0, L_x] \times [0, L_y] = [0, 2\pi a] \times [0, 2\pi a]$, where $a = 6371.22\,\mathrm{km}$ is the Earth radius, with bi-periodic boundary conditions. The gravity acceleration constant is set to $g = 9.80616\,\mathrm{ms}^{-2}$ and the Coriolis frequency constant is $f = 2\Omega$, with $\Omega = 7.292 \times 10^{-5}\,\mathrm{rad} \cdot \mathrm{s}^{-1}$. The mean depth is $\bar{\eta} = 10\,\mathrm{km}$ so that the gravity wave speed is $c = \sqrt{g\bar{\eta}} \approx 313\,\mathrm{ms}^{-1}$, hence similar to the speed of sound.

The experiments will be performed with a horizontal discretization of 512 spectral modes in each dimension. This corresponds to 768 physical grid points to avoid aliasing effects, which would result in a grid cell with a length of approximately 52 km in each coordinate. The exception is the reference solution (REF), for which we will use 1024 spectral modes per coordinate. Such high horizontal resolution was chosen in order to reduce the errors relative to spatial discretizations and allow a clearer comparison of the different time stepping schemes. The time step sizes will vary according to the analysis to be investigated.

We will present results of errors in two metrics: maximum absolute error (MaxError) and root mean square error (RMSError), always for fixed integration time (timestamp). In case of mismatching resolutions, where pointwise comparison does is not well defined, bi-cubic spline interpolation is used on the highest resolution result to obtain information on the lowest resolution grid. This lack of matching happens as we are using a collocated grid (A-grid in geophysical notation), with physical representation of the quantities considered in the center of the cell.

6.2. Kinetic energy spectra. The analysis of the energy spectra is deeply related to the study of turbulence in fluid dynamics models, which is well studied for the atmosphere (e.g. [33, 31]). Here, we do not intend to do turbulence analysis, but rather simply use spectrum analysis to compare how the different schemes act on small-scale waves. Therefore, we will assume a simplified kinetic energy spectrum analysis, avoiding structure functions and two-point correlation functions [43], as follows.

The two-dimensional kinetic energy spectrum will be obtained using the Fourier transformed velocities, with modes denoted as $(\hat{u}(\vec{k}), \hat{v}(\vec{k}))$, $\vec{k} = (k_1, k_2)$, with

$$E_{\vec{k}} = \frac{1}{2} \left(\hat{u}(\vec{k})\, \hat{u}^*(\vec{k}) + \hat{v}(\vec{k})\, \hat{v}^*(\vec{k}) \right), \tag{52}$$

where * represents the complex conjugate. One may now define the one-dimensional Discrete Power Density Spectra as [42]

$$E_n = \sum_{n \le \|\vec{k}\| < n+1} E_{\vec{k}}, \tag{53}$$

where $\|\vec{k}\| = \sqrt{k_1^2 + k_2^2}$, and E_k represents the spectrum density with respect to horizontal wavenumber n and wavelength L/n, where L is the size of the domain. This closely follows what is usually done in spherical atmospheric models (e.g. [31]).

6.3. Unstable jet test case. On the sphere, a well-known test case is defined by the Galewsky et al [21] initial conditions. These initial conditions are formed of 2 geostrophic balanced mid-latitude zonal jets. A small perturbation in the height field is added to generate fast gravity waves that eventually destabilize the jets and form well-defined vortices after a few days. On the bi-periodic plane, no such test case exists, so we propose something similar in the following way.

The jets are defined by the u and v velocities as,

$$u(x, y) = u_0 \left(\sin(2\pi y/L_y)\right)^{81}, \qquad v(x, y) = 0, \tag{54}$$

$u_0 = 50\text{ms}^{-1}$ is the maximum speed, the power of 81 was chosen so that the jet is confined in a small region, and it is built to ensure periodicity. To ensure that the depth field is in geostrophic balance with the velocity field, that is, that the initial conditions are analytically in a steady state, we define the depth perturbation as

$$\eta(x, y) = -\frac{f}{g} \int_0^y u(x, s) ds. \tag{55}$$

The integral is solved numerically through repeated piecewise Gaussian integrals ensuring that the integral is calculated within desired tolerance for double precision.

Small Gaussian perturbations (η_p) are added to η to trigger the barotropic instability,

$$\eta_p(x, y) = 0.01\bar{\eta} \left[\exp\{-kd_1(x, y))\} + \exp\{-kd_2(x, y)\}\right], \tag{56}$$

where $k = 1000$, and $d_i(x, y) = \frac{(x-x_i)^2}{L_x^2} + \frac{(y-y_i)^2}{L_y^2}$, $i = \{1, 2\}$, are the square Euclidean distances of (x, y) to the points $p_1 = (x_1, y_1) = (0.85L_x, 0.75L_y)$, $p_2 = (x_2, y_2) = (0.15L_x, 0.25L_y)$, respectively.

Initial conditions are presented in Figure 1. Note that the zonal jets move towards different directions (left-right), in order to ensure periodicity of all initial fields. We present in Figures 2 and 3 results from the high resolution reference scheme (REF) with a small time step size of 2 seconds. Figure 2 shows how the initial Gaussian perturbations trigger the generation of fast-moving inertia-gravity waves that dominate the initial period of time integration. The waves start interacting with each other through the nonlinear effects and eventually disturb the jets to form well-defined vortices at day 10, shown in Figure 3a with the vorticity of the flow.

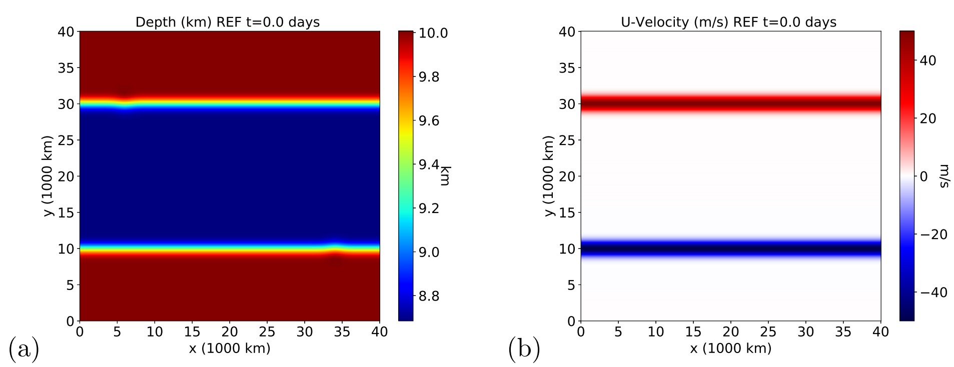

FIG. 1. *Initial condition for unstable jet test case. (a) Total depth ($\eta + \bar{\eta}$) and (b) zonal velocity (u).*

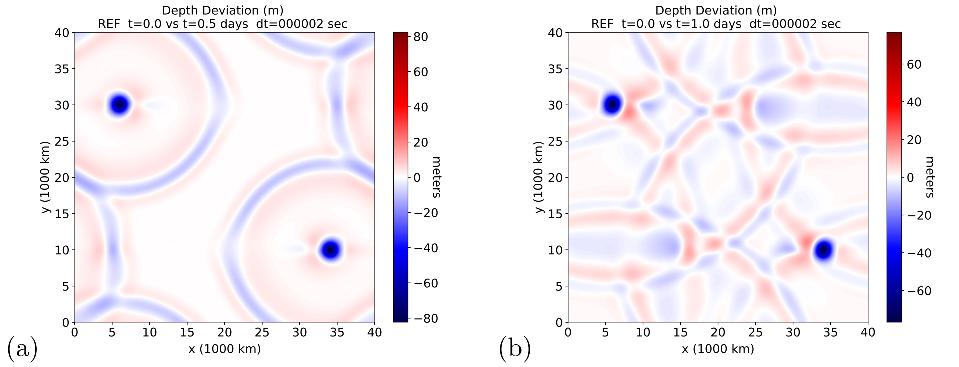

FIG. 2. *Reference solution (REF) for depth difference from initial conditions with respect to (a) half and (b) one days.*

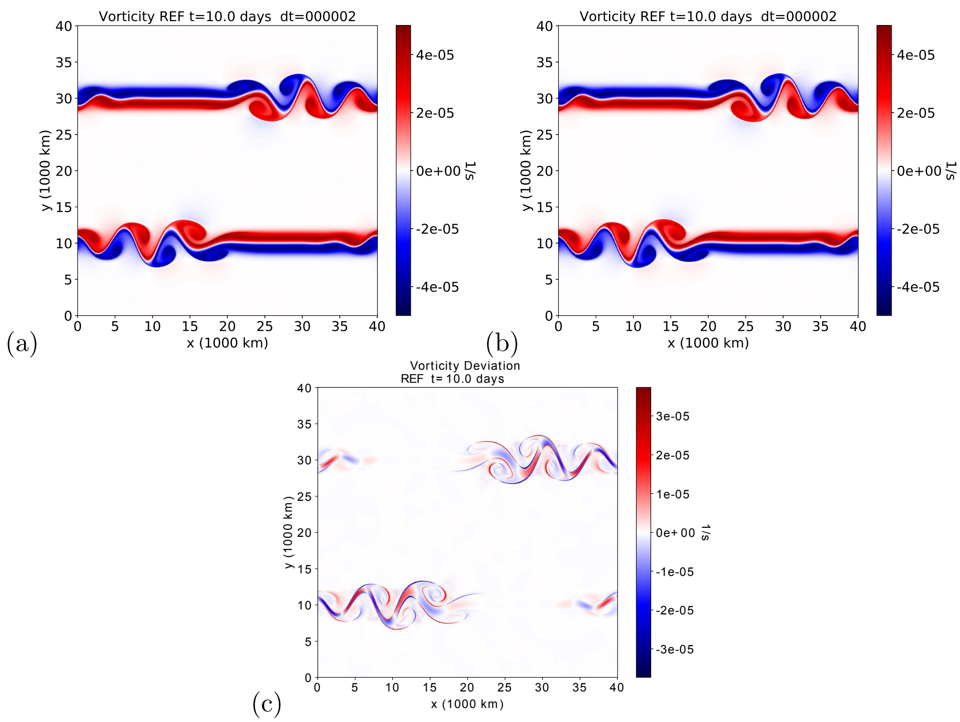

FIG. 3. *Reference solution for vorticity at 10 days. (a) Full nonlinear SWE. (b) SWE neglecting the nonlinear divergence term ($\tilde{\mathcal{N}} = 0$). (c) Difference between (a) and (b).*

We will also use this test case neglecting the nonlinear divergence of the SWE ($\tilde{\mathcal{N}}$ from equation (43)). The SWE flow is still nonlinear, due to the nonlinear advection term. In fact, the solution of the unstable jet initial condition neglecting the nonlinear divergence is very similar to the solution considering this term, as may be seen in Figure 3b. Even though this term might not visually influence much the solutions after 10 days (see Figure 3c), it plays an important role in energy cascade and nonlinear interaction of waves. Also, it will influence the numerical properties of the scheme, as we will see further on in the next section.

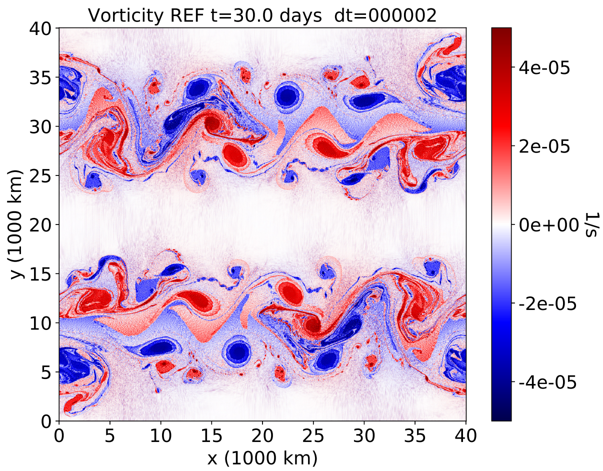

FIG. 4. *Reference solution for vorticity at 30 days using the full nonlinear SWE.*

After longer periods of time, the flow goes on to develop into a fully turbulent flow, as may be seem in Figure 4 (the flow considering $\tilde{\mathcal{N}} = 0$ is very similar to the full SWE). From a spectral point of view, energy moves towards smaller wavelengths as time evolves, as may be seen in Figure 5. The initial kinetic energy spectrum is basically defined by the spectrum of powers of trigonometric functions (in this case $\sin^{81}(2\pi y/L_y)$). As the power chosen (81) is odd, the spectrum will be zero for all even wavenumbers. That is why we see a zig-zag pattern in the early stages of integration in the kinetic energy spectrum. Energy builds up in even wavenumbers due to nonlinear interactions. Note also that the spectra converges towards the well known $-5/3$ power law of 2D kinetic energy turbulence [33]. Reproducing this kind of spectra in small wavelengths stably is usually a major challenge for numerical schemes.

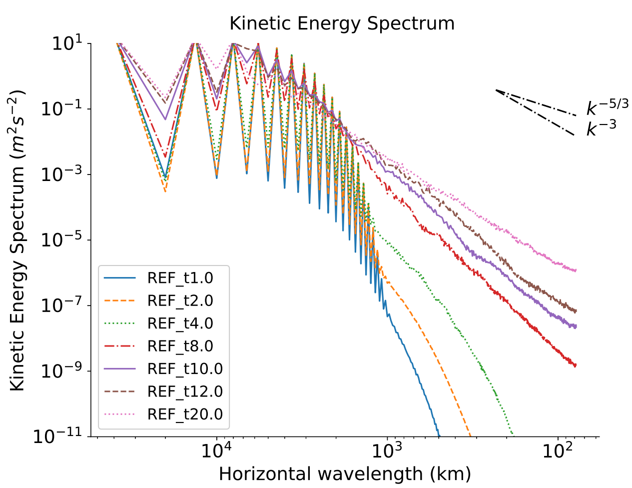

FIG. 5. *Kinetic energy spectrum for reference solution using the full nonlinear SWE for different integration times (from 1 day to 20 days).*

6.4. Analysis of Shallow Water Equations without nonlinear divergence. Considering $\tilde{\mathcal{N}} = 0$ simplifies the semi-Lagrangian exponential schemes. In fact, in this case, SL-EXP-SETTLS and SL-ETD2RK are equivalent, since the only non-linearity left (advection) is treated within the semi-Lagrangian approach. SL-SI-SETTLS also greatly simplifies for similar reasons. RK-FDC, ETD2RK and REF still have to deal with the nonlinear advection as a nonlinear term. The finite differences scheme RK-FDC is built about the vector invariant form of the equations, where nonlinear advection is not explicit, therefore it is not clear how to remove the nonlinear divergence and we do not present results of this scheme for this SWE without nonlinear divergence.

The initial period is dominated by linear gravity waves, so that is where we expect to see benefits of the exponential integration scheme with respect to the semi-implicit scheme. We show in Figure 6 the errors at day 1 of integration for the unstable jet test case without nonlinear divergence. A few remarks are relevant at this point. First, as stated before, SL-EXP-SETTLS and SL-ETD2RK are equivalent in this case. Also, it should be noted that a fixed horizontal resolution was used in these tests, therefore, for small time step sizes, the dominating error becomes the spatial interpolation errors. Increasing the resolution reduces the errors of the semi-Lagrangian schemes. Therefore, at small time steps, ETD2RK is much more accurate than the other schemes, since all spatial operators are treated spectrally. However, the semi-Lagrangian schemes are stable throughout all time step sizes tested, whereas the ETD2RK scheme is limited by advection CFL time step size. In general, the semi-Lagrangian exponential schemes are more accurate than the semi-implicit scheme (SL-SI-SETTLS), due to the more accurate treatment of the linear waves. Concluding, the semi-Lagrangian exponential schemes provide a more accurate way, compared to SL-SI-SETLLS, to extend the time step size allowed by the traditional exponential scheme (ETD2RK).

Due to the dynamically unstable nature of the test case, quantitative analysis of errors in longer periods of time is not usually indicated. However, it is interesting to see qualitatively how the schemes behave once the vortices have developed. We show in Figure 7 the vorticity at day 10 for the several schemes investigated. All schemes seem to be able to represent well the vortex formation, but we notice that the ETD2RK has more noise at or around the vortices, whereas the semi-Lagrangian schemes show smoother vortices, due to the successive non-spectral interpolations required. With a time step size of 450 seconds, the ETD2RK scheme is unstable, but the semi-Lagrangian schemes produce high-quality solutions (see Figure 8).

6.5. Analysis of the Full Shallow Water Equations. In this section, we will analyze the schemes with respect to the full SWE, including the nonlinear divergence. In this case, the RK-FDC schemes will also be included in the analysis. Also, the different semi-Lagrangian exponential schemes (SL-ETD2RK and SL-EXP-SETTLS) now differ from each other.

We show in Figure 9 the errors associated with the integration of the full SWE for the unstable jet test case at day 1. As in the previous test, due to the limitation imposed by the spatial interpolation used in the semi-Lagrangian schemes, the ETD2RK scheme provides more accurate results when small time step sizes are used. The ETD2RK scheme is again limited by CFL condition for advection. The RK-FDC scheme is limited in both time and space: the finite differences scheme limits the accuracy, and the gravity wave speed CFL limits the time step size. With the inclusion of the nonlinear divergence, the SL-EXP-SETTLS scheme turns out to be

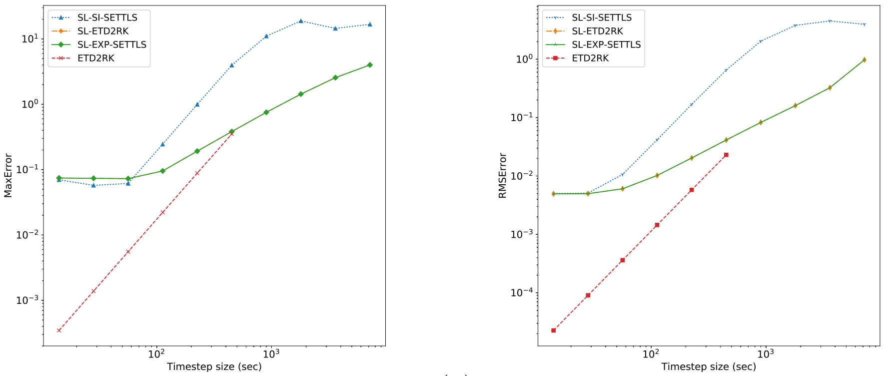

(a) (b)

Fig. 6. *For each scheme, the (a) maximum absolute error and the (b) root mean square error for 1 integration day with respect to the reference are shown for different time step sizes. All schemes were tested for all time step sizes indicated. If a scheme does not shows a value for a large time step it indicates it became unstable for this test. The SWE without nonlinear divergence were adopted in this test, therefore SL-EXP-SETTLS and SL-ETD2RK are identical.*

unstable when used with large time steps. Compared to the SL-SI-SETTLS scheme, the SL-EXP-SETTLS does not damp the high wavenumber gravity waves, which interact with each other in the nonlinear divergence and becomes numerically unstable. Differently, the SL-ETD2RK scheme is stable with large time steps, and is more accurate than the SL-SI-SETTLS scheme, due to the more accurate treatment of the linear waves. The theoretical stability analysis of the semi-Lagrangian schemes is still a matter to be investigated and is here considered only in an empirical sense. However, we point out an important difference between them: SL-EXP-SETTLS is a multistep scheme (requires an extrapolation from a previous time step), whereas the SL-ETD2RK is a single step method (apart for the extrapolation used in the back trajectory calculation).

From Figure 9 we again notice that SL-ETD2RK seems to be a viable extension of the ETD2RK scheme to larger time steps, being more accurate than the SL-SI-SETTLS. In Figure 10 we show the vorticity field at day 10 for 3 different schemes (SL-SI-SETTLS, SL-EXP-ETD2RK, and ETD2RK). They are again qualitatively very similar, although the ETD2RK shows more high wavenumber oscillations around the vortices. Interestingly, for larger time step sizes, due to the extra energy in the high wavenumber gravity waves, the SL-ETD2RK triggers small turbulent like features after long runs when compared to SL-SI-SETTLS. This is illustrated in figure 11b. Since there is no dissipation of near grid scale energy, this energy destabilizes the jet into smaller scale features. This is clearly seen in Figure 12, where we also notice that the ETD2RK scheme has more energy in the smaller scales.

6.6. Shallow Water Equations with term specific viscosity. For the purpose of weather and climate simulations, a certain amount of small-scale dissipation is usually required, either from a numerical stability perspective or from a physical point of view. The SL-SI-SETTLS scheme, when used in the full IFS dynamical core, adopts a spectral hyper-viscosity filter in the momentum equations in order to both numerically stabilize the scheme and physically dissipate energy from the small-scale

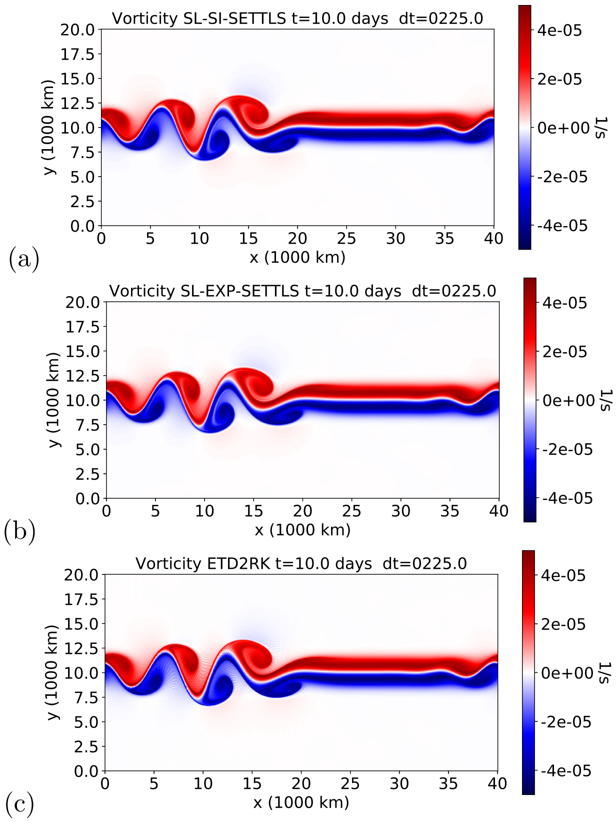

FIG. 7. *Numerical solution of the SWE without nonlinear divergence for the unstable jet test case at time 10 days for the vorticity field using a time step size of 225 seconds. (a) SL-SI-SETTLS, (b) SL-EXP-SETTLS (which is identical to SL-ETD2RK), (c) ETD2RK.*

energy tail (see [24] for an analysis of the impacts of the viscosity in a global spectral model). We remark that in full models this energy in high wavenumbers could be used to model physical sub-grid properties, such as convection.

With the semi-Lagrangian exponential scheme, it is possible to preserve the linear waves precise dispersion and apply a term specific dissipation in the nonlinear divergence term. This way, linear waves (long and short) are treated accurately, but only the longer waves originated from their nonlinear interaction are preserved in the model. This allows the model to be numerically stable without damping the linear waves, and also provides dissipation of small-scale features generated by the additional energy in high wavenumbers excited by the exponential integration.

In the analysis that follows we considered an implicit spectral diffusion applied only to the nonlinear divergence term. Let $c_{\vec{k}}$ be the Fourier coefficient with wavenumbers $\vec{k} = (k_1, k_2)$, then the implicit diffusion is such that the coefficient is filtered to

$$\tilde{c}_{\vec{k}} = \frac{c_{\vec{k}}}{1 + \Delta t\, \mu \|\vec{k}\|^2}, \tag{57}$$

where μ is a diffusion coefficient, Δt is the time step size and we are assuming normalized wavenumbers (adjusted for the domain size).

We start by analyzing, with different viscosities, the kinetic energy spectrum of

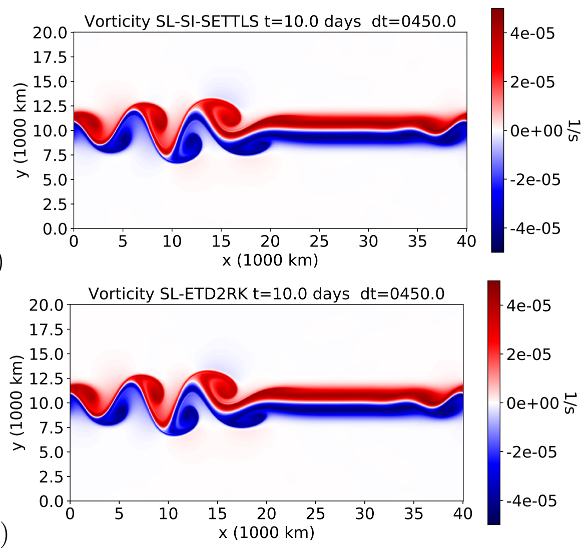

(a)

(b)

Fig. 8. *Numerical solution of the SWE without nonlinear divergence at time 10 days for the vorticity field using a time step size of 450 seconds. (a) SL-SI-SETTLS, (b) SL-EXP-SETTLS (which is identical to SL-ETD2RK). The scheme ETD2RK is not shown as it is unstable for this time step size.*

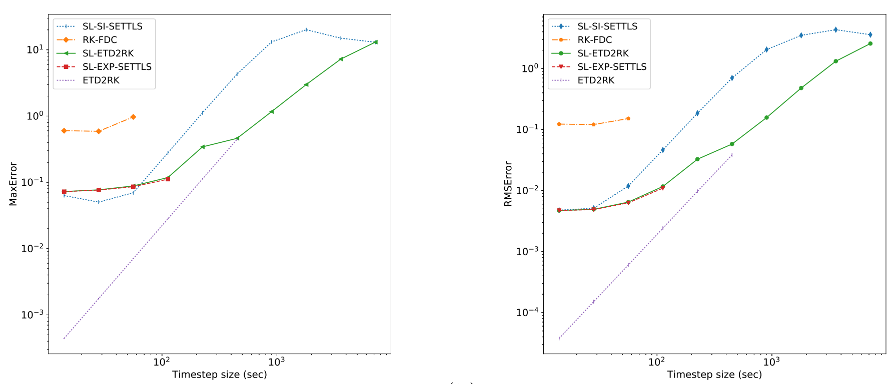

(a) (b)

Fig. 9. *For each scheme, the (a) maximum absolute error and the (b) root mean square error for 1 integration day with respect to the reference are shown for different time step sizes. All schemes were tested for time step sizes indicated. If a scheme does not shows a value for a large time step it indicates it became unstable for this test. The full SWE were adopted in this test.*

the semi-Lagrangian ETD2RK scheme. Figure 13 shows how the amount of viscosity required to obtain a solution along the lines of the SL-SI-SETTLS with a time step size of 900 seconds, and, following these results, we will adopt $\mu = 25.6 \times 10^6\,\mathrm{m}^2\mathrm{s}^{-1}$. This value is similar to what is actually used in weather forecasting systems for the full equations, whereas here, we are only considering it for the nonlinear divergence (see [32] for a comprehensive discussion on the use of diffusion in atmospheric models).

Figure 14 shows results of the vorticity field after 10 days. The SL-ETD2RK

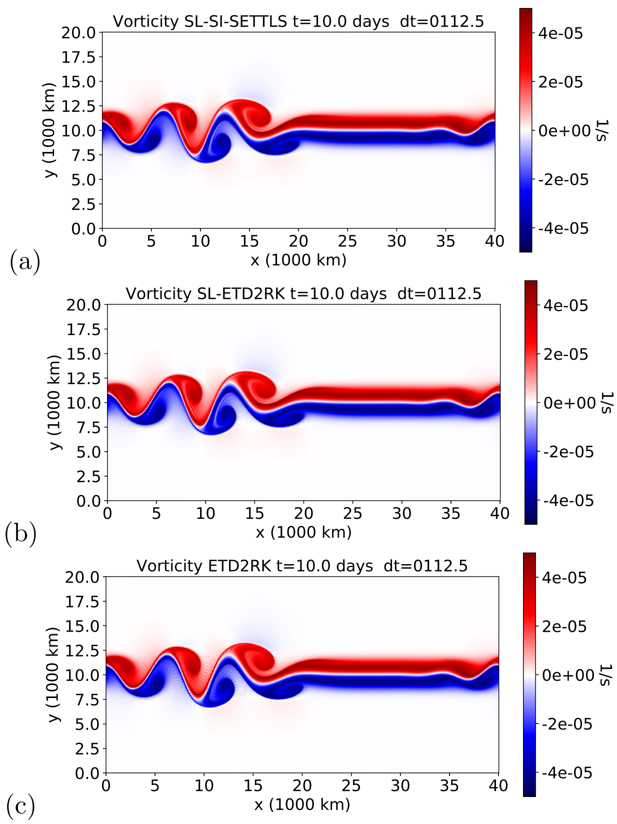

FIG. 10. *Numerical solution of the Full SWE for the unstable jet test case at time 10 days for the vorticity field using a time step size of 112.5 seconds. (a) SL-SI-SETTLS, (b) SL-EXP-ETD2RK, (c) ETD2RK.*

scheme now does not develop near grid scale features even with a time step size of 900 seconds. Even with the implicit diffusion, the ETD2RK scheme is still not able to do time step sizes as large as the semi-Lagrangian schemes, due to the instability originated from the nonlinear advection term. To stabilize the ETD2RK scheme, further terms should be damped, which would likely reduce the accuracy of the scheme. As before, the SL-EXP-SETTLS scheme is unstable for large time steps.

Error results at day 1 of integration are shown in Figure 15, where we can see that now the two semi-Lagrangian exponential schemes deliver more accuracy compared to the SL-SI-SETTLS scheme.

7. Concluding remarks. This paper is intended to be a proof of concept for a novel approach that combines semi-Lagrangian and exponential integration techniques. The approach may be helpful for users of standard exponential integration techniques as a way to allow larger time step sizes preserving accurate solutions. In this case, one might even wish to use a higher order semi-Lagrangian scheme, such as the one proposed in [10]. For the application perspective, considering weather and climate models, the method presents a way to improve the dispersion properties of well-established schemes, therefore better representing linear fast gravity waves.

The results presented in this paper show the potential benefits of such a combination of different approaches. However, we do not present results in terms of

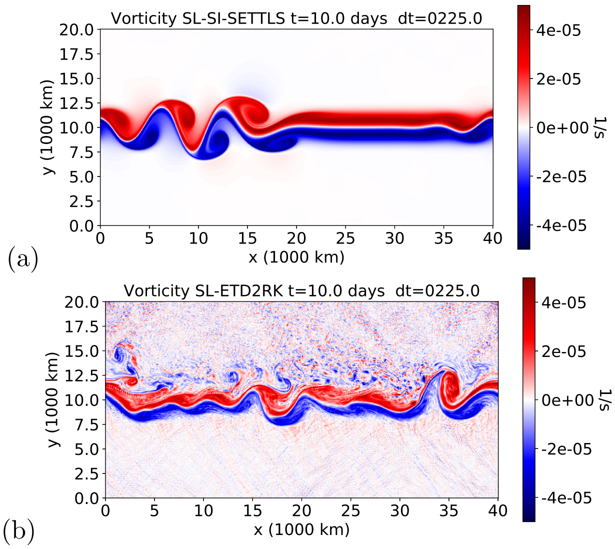

FIG. 11. *Numerical solution of the Full SWE at time 10 days for the vorticity field using a time step size of 225 seconds. (a) SL-SI-SETTLS, (b) SL-ETD2RK.*

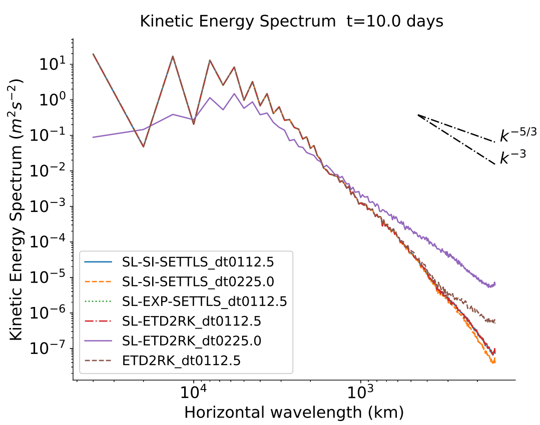

FIG. 12. *Kinetic energy spectrum for different methods and time step sizes for the full nonlinear SWE at day 10 of integration.*

computational performance of the schemes discussed. We intend to present results of the computational workload of the approach in a later publication showing results in a more realistic setup, considering the spherical SWE. In this case, we do not explicitly have the exponential of the linear operator easily accessible. Therefore, this analysis will highly depend on how the matrix exponential is calculated, so it goes beyond the scope of this paper.

Acknowledgements. The ideas behind this work originated from discussions with Colin Cotter, Jemma Shipton and Beth Wingate, whom are greatly acknowledged. We would also like to thank Saulo Barros for discussions with respect to

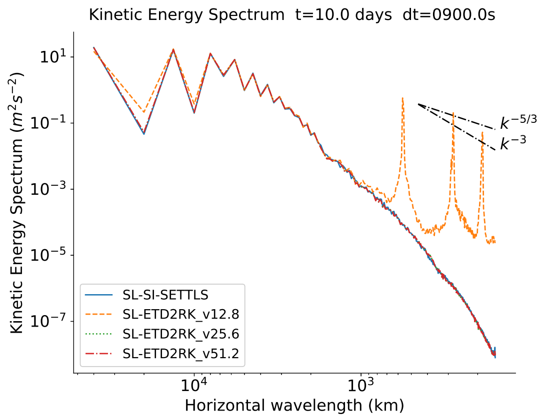

FIG. 13. *Kinetic energy spectrum considering an implicit diffusion on the nonlinear divergence term with* $\mu = 12.8 \times 10^6\ \mathrm{m^2s^{-1}}$, $\mu = 25.6 \times 10^6\ \mathrm{m^2s^{-1}}$ *and* $\mu = 51.2 \times 10^6\ \mathrm{m^2s^{-1}}$ *for the SL-ETD2RK scheme and no diffusion for the SL-SI-SETTLS scheme.*

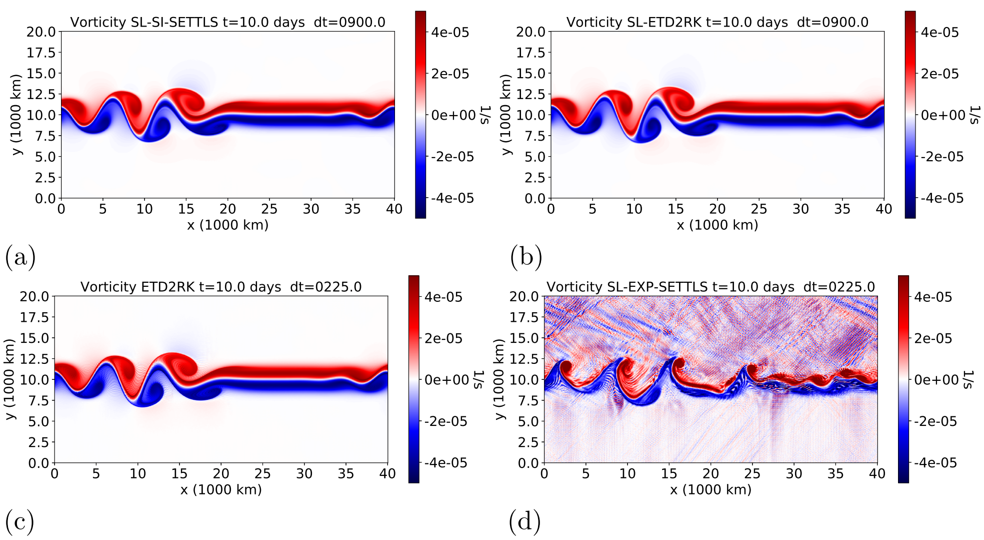

FIG. 14. *Numerical solution of the Full SWE at time 10 days for the vorticity field using implicit diffusion on the nonlinear divergence term with* $\mu = 25.6 \times 10^6\ \mathrm{m^2s^{-1}}$. *(a) SL-SI-SETTLS with* $\Delta t = 900s$, *(b) SL-ETD2RK with* $\Delta t = 900s$, *(c) ETD2RK with* $\Delta t = 225s$, *(d) SL-ETD2RK with* $\Delta t = 225s$.

semi-Lagrangian spectral schemes.

Appendix A. Properties of semi-Lagrangian exponential schemes and pitfalls.

A.1. Commutation of linear operator and interpolation on departure points. Consider a general vector $\vec{w} \in \mathbb{R}^n$, a linear operator $T \in \mathbb{R}^n \times \mathbb{R}^n$, which will represent here, for example, a matrix exponential, and $\mathcal{I}_{\vec{x}} : \mathbb{R}^n \to \mathbb{R}^n$ an interpolation operation with respect to points $\vec{x} \in \mathbb{R}^n$. Following the semi-Lagrangian notation for interpolation, we may concisely write that $\mathcal{I}_{\vec{x}}(\vec{w}) = \vec{w}_*$, where the $_*$ implicitly indicates the interpolation with respect to $\vec{x}$. This subsection is just to point a simple example to illustrate that even in very simple cases $(T\vec{w})_* \neq T(\vec{w}_*)$.

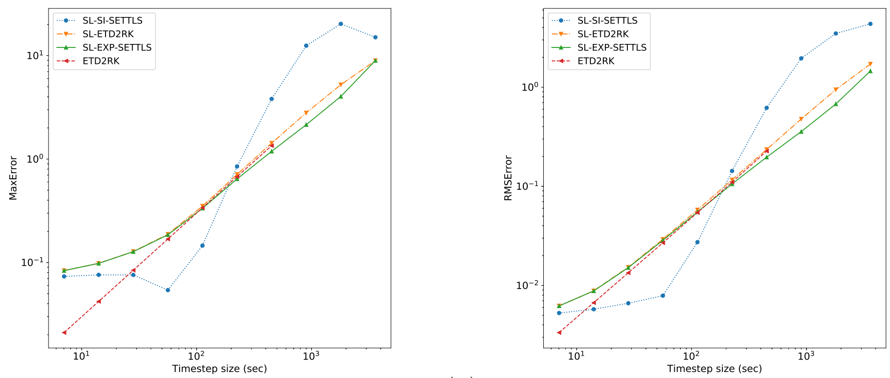

(a) (b)

FIG. 15. *Adopting a implicit diffusion on the nonlinear divergence term with* $\mu = 25.6 \times 10^6\,\mathrm{m^2s^{-1}}$, *for each scheme, the (a) maximum absolute error and the (b) root mean square error for 1 integration day with respect to the reference are shown for different time step sizes. All schemes were tested for time step sizes indicated. If a scheme does not shows a value for a large time step it indicates it became unstable for this test. The full SWE were adopted in this test.*

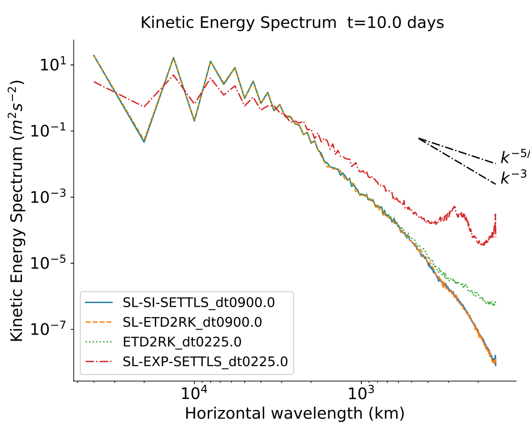

FIG. 16. *Kinetic energy spectrum considering an implicit diffusion on the nonlinear divergence term with* $\mu = 25600000\,\mathrm{m^2s^{-1}}$, *for the schemes/parameters shown in Figure 15*

Consider a 1D periodic grid with uniformly spaced points $(x_i)_{i=1,n}$, with distance Δx from each other. In this example we will consider a scalar advection with constant velocity given by $\Delta x/\Delta t$, so that, after one time step, the departure points will be a simple translation and will match exactly their left neighbours. That is, the trajectory goes from t_n to t_{n+1} carrying the function value at x_{i-1} to the x_i point. In this case, the interpolation to departure points will be given by a periodic shift in the indexes,

$$\mathcal{I}_{\vec{x}}(\vec{w}) = \mathcal{I}_{\vec{x}}([w_1, w_2, w_3, \dots, w_n]) = [w_n, w_1, w_2, \dots, w_{n-1}] = \vec{w}_*. \tag{58}$$

Note that the operator $\mathcal{I}_{\vec{x}}$ is a linear operator.

Now consider a simple diagonal linear operator $T = (\alpha_{ii})_{i=1,n}$, with $\alpha_{ii} \neq \alpha_{jj}$, for $j \neq i$. In this case,

$$(T\vec{w})_* = ([\alpha_{11}w_1, \alpha_{22}w_2, w_3, \dots, \alpha_{nn}w_n])_* \\ = [\alpha_{nn}w_n, \alpha_{11}w_1, \alpha_{22}w_2, w_3, \dots, \alpha_{(n-1)(n-1)}w_{n-1}], \tag{59}$$

but

$$T(\vec{w}_*) = T[w_n, w_1, w_2, \dots, w_{n-1}] = [\alpha_{11}w_n, \alpha_{22}w_1, \dots, \alpha_{nn}w_{n-1}]. \tag{60}$$

Therefore, even if the trajectories are constant (or linear), the commutation does not generally hold.

In the more general case treated in the derivation of the semi-Lagrangian exponential scheme, the trajectories are nonlinear. Also, the linear operator is not necessarily diagonal, but one could think of its diagonalized version in complex space in a similar way, for which the terms in the diagonal would be the eigenvalues of the operator.

A.2. Approximation of an integral along trajectories. In this subsection we discuss approximations to

$$\int_{t_n}^{t_{n+1}} T(s)w(s, \vec{r}(s))ds \tag{61}$$

where $T : \mathbb{R} \to \mathbb{R}^n \times \mathbb{R}^n$, $w : \mathbb{R} \times \mathbb{R}^n \to \mathbb{R}^n$ and $\vec{r} : \mathbb{R} \to \mathbb{R}^n$ defines a characteristic path (trajectory) in $\mathbb{R}^n$, all being sufficiently smooth (at least continuous).

An approximation of the integral to midpoint of the trajectory would have the following form

$$A_1 = \Delta t[T(s)w(s, \vec{r}(s))]_{t_{n+1/2}}, \tag{62}$$

which, assuming a trajectory calculated exactly, would have an error of the order $\mathcal{O}(\Delta t^3)$. In semi-Lagrangian schemes the exact value of the functions (w) at trajectory midpoints are usually not known, so they are extrapolated and/or interpolated from values at fixed time steps. Let $v(s) = T(s)w(s, \vec{r}(s))$, and consider an interpolation/extrapolation of v as

$$A_1 \approx \mathcal{I}_{\vec{x}_{t_n}, \vec{x}_{t_{n+1}}}(v) = \mathcal{I}_{\vec{x}_{t_n}, \vec{x}_{t_{n+1}}}(Tw), \tag{63}$$

where we note that $\mathcal{I}$ depends on the arrival ($\vec{x}_{t_{n+1}}$) and departure points ($\vec{x}_{t_n}$) for the calculation of Tw, as was the case for the SETTLS scheme, for example.

On the other hand, as noticed in the previous subsection, T will not in general commute with $\mathcal{I}$. As a consequence, assuming $T(t)$ is known for all times, if one takes the approximation of the integral as

$$A_2 = \Delta t T(t_{n+1/2})w(t_{n+1/2}, \vec{r}(t_{n+1/2})), \tag{64}$$

and applies the interpolation/extrapolation only on w, to obtain

$$A_2 \approx \Delta t T(t_{n+1/2})\mathcal{I}_{\vec{x}_{t_n}, \vec{x}_{t_{n+1}}}(w), \tag{65}$$

the resulting approximation differs from the former ($A_1 \neq A_2$), with, for example, the operators used in the previous subsection. Interestingly, this may even be different if T does not vary in time.

Clearly, both approximations A_1 and A_2 are approximations to the desired integral with the same accuracy order. However, in a more general case, the midpoints of the trajectories may not coincide with regular grid points. As a result, A_2 may not always well defined, for example when T is formed by linear differential operators.

Appendix B. Semi-Lagrangian semi-implicit spectral scheme.

One of our reference methods is the scheme used in the IFS model, adapted to the SWE on the plane, that uses semi-Lagrangian semi-implicit time stepping with spectral horizontal discretization. This scheme, based on [29], is briefly described here for completeness.

The semi-implicit discretization with semi-Lagrangian Crank-Nicolson time stepping is based on the discretization described in Section 3.3. Substituting the SWE in this formulation we obtain an implicit linear differential system of the form

$$\alpha u^{n+1} - f v^{n+1} + g\eta_x^{n+1} = (\alpha u^n + f v^n - g\eta_x^n)_* \tag{66}$$

$$f u^{n+1} + \alpha f v^{n+1} + g\eta_y^{n+1} = (\alpha v^n - f u^n - g\eta_y^n)_* \tag{67}$$

$$\bar{\eta} u_x^{n+1} + \bar{\eta} v_y^{n+1} + \alpha\eta = (\alpha\eta^n - \bar{\eta}\delta^n)_* - 2\widetilde{(\eta\delta)}^{n+1/2} \tag{68}$$

where $\alpha = 2/\Delta t$, the $n+1/2$ term with $\widetilde{\cdot}$ is calculated using the SETTLS extrapolation and $\delta^n = u_x^n + v_y^n$ is the velocity divergence. The right-hand-side of the above equations are respectively denoted as (R_u^n, R_v, R_η^n). Writing (u, v) in terms of η as

$$\begin{pmatrix} u \\ v \end{pmatrix}^{n+1} = \frac{1}{\kappa}\begin{pmatrix} \alpha & f \\ -f & \alpha \end{pmatrix}\begin{pmatrix} R_u \\ R_v \end{pmatrix}^n - \frac{g}{\kappa}\begin{pmatrix} \alpha & f \\ -f & \alpha \end{pmatrix}\begin{pmatrix} \eta_x \\ \eta_y \end{pmatrix}^{n+1} \tag{69}$$

with $\kappa = \alpha^2 + f^2$, and applying the divergence and vorticity operations to $(u, v)^{n+1}$, we obtain a single Helmholtz equation for η as

$$\kappa\eta^{n+1} - g\bar{\eta}\nabla^2\eta^{n+1} = -\bar{\eta}R_\delta^n - \bar{\eta}\frac{f}{\alpha}R_\zeta^n + \frac{\kappa}{\alpha}R_\eta^n, \tag{70}$$

where $R_\delta^n = \partial_x R_u^n + \partial_y R_v^n$ and $R_\zeta^n = \partial_x R_v^n - \partial_y R_u^n$ are respectively the divergence and vorticity of (R_u^n, R_v^n). This equation can be easily solved in spectral space, since the Fourier basis define eigenfunctions of the linear differential operators. Once η^{n+1} is obtained, (u^{n+1}, v^{n+1}) is obtained via (69).

REFERENCES

[1] J. D. Anderson and J. Wendt, *Computational fluid dynamics*, vol. 206, Springer, 1995.

[2] A. Arakawa and V. Lamb, *Computational design of the basic dynamical processes of the UCLA general circulation model*, Methods in Computational Physics, 17 (1977), pp. 173–265.

[3] R. K. Archibald, K. J. Evans, J. Drake, and J. White, *Time acceleration methods for advection on the cubed sphere*, in International Conference on Computational Science, Springer, 2009, pp. 253–262.

[4] S. R. M. Barros, D. Dent, L. Isaksen, G. Robinson, G. Mozdzynski, and F. Wollenweber, *The IFS model: A parallel production weather code*, Parallel Computing, 21 (1995), pp. 1621–1638.

[5] P. Bartello and S. J. Thomas, *The cost-effectiveness of semi-Lagrangian advection*, Monthly weather review, 124 (1996), pp. 2883–2897.

[6] J. Bates, F. Semazzi, R. Higgins, and S. R. Barros, *Integration of the shallow water equations on the sphere using a vector semi-lagrangian scheme with a multigrid solver*, Monthly Weather Review, 118 (1990), pp. 1615–1627.

[7] G. Beylkin, J. M. Keiser, and L. Vozovoi, *A new class of time discretization schemes for the solution of nonlinear PDEs*, Journal of Computational Physics, 147 (1998), pp. 362–387.

[8] E. Carr, I. Turner, and P. Perr, *A variable-stepsize jacobian-free exponential integrator for simulating transport in heterogeneous porous media: Application to wood drying*, Journal of Computational Physics, 233 (2013), pp. 66 – 82.

[9] E. Celledoni, *Eulerian and semi-Lagrangian schemes based on commutator-free exponential integrators*, Group theory and numerical analysis, 39 (2005), pp. 77–90.

[10] E. Celledoni and B. K. Kometa, *Semi-Lagrangian Runge-Kutta exponential integrators for convection dominated problems*, Journal of Scientific Computing, 41 (2009), pp. 139–164.

[11] E. Celledoni, B. K. Kometa, and O. Verdier, *High order semi-Lagrangian methods for the incompressible Navier–Stokes equations*, Journal of Scientific Computing, 66 (2016), pp. 91–115.

[12] C. Clancy and P. Lynch, *Laplace transform integration of the shallow-water equations. Part II: Semi-Lagrangian formulation and orographic resonance*, Quarterly Journal of the Royal Meteorological Society, 137 (2011), pp. 800–809.

[13] C. Clancy and J. A. Pudykiewicz, *On the use of exponential time integration methods in atmospheric models*, Tellus A: Dynamic Meteorology and Oceanography, 65 (2013), p. 20898.

[14] S. M. Cox and P. C. Matthews, *Exponential time differencing for stiff systems*, Journal of Computational Physics, 176 (2002), pp. 430–455.

[15] M. Diamantakis, *The semi-Lagrangian technique in atmospheric modelling: current status and future challenges*, in ECMWF Seminar in numerical methods for atmosphere and ocean modelling, 2013, pp. 183–200.

[16] T. Dubos, S. Dubey, M. Tort, R. Mittal, Y. Meurdesoif, and F. Hourdin, *DYNAMICO-1.0, an icosahedral hydrostatic dynamical core designed for consistency and versatility*, Geoscientific Model Development, 8 (2015), pp. 3131–3150.

[17] D. R. Durran, *Numerical methods for fluid dynamics: With applications to geophysics*, vol. 32, Springer, 2010.

[18] ECMWF, *PART III: DYNAMICS AND NUMERICAL PROCEDURES*, IFS Documentation, ECMWF, 2017, ch. ., p. .

[19] M. Falcone and R. Ferretti, *Convergence analysis for a class of high-order semi-lagrangian advection schemes*, SIAM Journal on Numerical Analysis, 35 (1998), pp. 909–940.

[20] S. N. Figueroa, J. P. Bonatti, P. Y. Kubota, G. A. Grell, H. Morrison, S. R. Barros, J. P. Fernandez, E. Ramirez, L. Siqueira, G. Luzia, et al., *The Brazilian global atmospheric model (BAM): performance for tropical rainfall forecasting and sensitivity to convective scheme and horizontal resolution*, Weather and Forecasting, 31 (2016), pp. 1547–1572.

[21] J. Galewsky, R. K. Scott, and L. M. Polvani, *An initial-value problem for testing numerical models of the global shallow-water equations*, Tellus A, 56 (2004), pp. 429–440.

[22] F. Garcia, L. Bonaventura, M. Net, and J. Sánchez, *Exponential versus IMEX high-order time integrators for thermal convection in rotating spherical shells*, Journal of Computational Physics, 264 (2014), pp. 41–54.

[23] S. Gaudreault and J. A. Pudykiewicz, *An efficient exponential time integration method for the numerical solution of the shallow water equations on the sphere*, Journal of Computational Physics, 322 (2016), pp. 827 – 848.

[24] A. Gelb and J. P. Gleeson, *Spectral viscosity for shallow water equations in spherical geometry*, Monthly Weather Review, 129 (2001), pp. 2346–2360.

[25] T. Haut, T. Babb, P. Martinsson, and B. Wingate, *A high-order time-parallel scheme for solving wave propagation problems via the direct construction of an approximate time-evolution operator*, IMA Journal of Numerical Analysis, (2015), p. drv021.

[26] M. Hochbruck and C. Lubich, *On Krylov subspace approximations to the matrix exponential operator*, SIAM Journal on Numerical Analysis, 34 (1997), pp. 1911–1925.

[27] M. Hochbruck and A. Ostermann, *Exponential integrators*, Acta Numerica, 19 (2010), pp. 209–286.

[28] J. R. Holton, *An introduction to dynamic meteorology*, Academic Press, 4 ed., 2004.

[29] M. Hortal, *The development and testing of a new two-time-level semi-lagrangian scheme (settls) in the ecmwf forecast model*, Quarterly Journal of the Royal Meteorological Society, 128 (2002), pp. 1671–1687.

[30] G. L. Kooij, M. A. Botchev, and B. J. Geurts, *An Exponential Time Integrator for the Incompressible Navier–Stokes Equation*, SIAM Journal on Scientific Computing, 40 (2018), pp. B684–B705.

[31] J. N. Koshyk and K. Hamilton, *The horizontal kinetic energy spectrum and spectral budget*

simulated by a high-resolution troposphere–stratosphere–mesosphere GCM, Journal of the Atmospheric Sciences, 58 (2001), pp. 329–348.

[32] P. H. Lauritzen, C. Jablonowski, M. A. Taylor, and R. D. Nair, *Numerical techniques for global atmospheric models*, vol. 80, Springer Science & Business Media, 2011.

[33] E. Lindborg, *Can the atmospheric kinetic energy spectrum be explained by two-dimensional turbulence?*, Journal of Fluid Mechanics, 388 (1999), pp. 259–288.

[34] J. Loffeld and M. Tokman, *"comparative performance of exponential, implicit, and explicit integrators for stiff systems of odes"*, Journal of Computational and Applied Mathematics, 241 (2013), pp. 45 – 67.

[35] A. Majda, *Introduction to PDEs and Waves for the Atmosphere and Ocean*, vol. 9, American Mathematical Soc., 2003.

[36] A. McDonald, *Accuracy of Multiply-Upstream Semi-Lagrangian Advective Schemes II*, Mon. Wea. Rev., 115 (1987), pp. 1446–1450.

[37] C. McLandress, *On the importance of gravity waves in the middle atmosphere and their parameterization in general circulation models*, Journal of Atmospheric and Solar-Terrestrial Physics, 60 (1998), pp. 1357–1383.

[38] G. Mengaldo, A. Wyszogrodzki, M. Diamantakis, S.-J. Lock, F. X. Giraldo, and N. P. Wedi, *Current and Emerging Time-Integration Strategies in Global Numerical Weather and Climate Prediction*, Archives of Computational Methods in Engineering, (2018), pp. 1–22.

[39] C. Moler and C. Van Loan, *Nineteen dubious ways to compute the exponential of a matrix, twenty-five years later*, SIAM review, 45 (2003), pp. 3–49.

[40] P. S. Peixoto and S. R. Barros, *On vector field reconstructions for semi-lagrangian transport methods on geodesic staggered grids*, J. Comput. Phys., 273 (2014), pp. 185 – 211.

[41] O. Pironneau, *On the transport-diffusion algorithm and its applications to the Navier-Stokes equations*, Numerische Mathematik, 38 (1982), pp. 309–332.

[42] F. Plunian, R. Stepanov, and P. Frick, *Shell models of magnetohydrodynamic turbulence*, Physics Reports, 523 (2013), pp. 1–60.

[43] S. B. Pope, *Turbulent flows*, 2001.

[44] M. K. Rajpoot, S. Bhaumik, and T. K. Sengupta, *Solution of linearized rotating shallow water equations by compact schemes with different grid-staggering strategies*, Journal of Computational Physics, 231 (2012), pp. 2300–2327.

[45] D. A. Randall, *Geostrophic Adjustment and the Finite-Difference Shallow-Water Equations*, Mon. Wea. Rev., 122 (1994), pp. 1371–+.

[46] H. Ritchie, *Application of the semi-lagrangian method to a spectral model of the shallow water equations*, Mon. Wea. Rev., 116 (1988), pp. 1587–1598.

[47] A. Robert, *A stable numerical integration scheme for the primitive meteorological equations*, Atmosphere-Ocean, 19 (1981), pp. 35–46.

[48] A. Robert, *A semi-Lagrangian and semi-implicit numerical integration scheme for the primitive meteorological equations*, Journal of the Meteorological Society of Japan. Ser. II, 60 (1982), pp. 319–325.

[49] R. Sadourny, *The dynamics of finite-difference models of the shallow-water equations*, Journal of the Atmospheric Sciences, 32 (1975), pp. 680–689.

[50] M. Schreiber and R. Loft, *A parallel time-integrator for solving the linearized shallow water equations on the rotating sphere*, under revision in Numer. Linear Algebra Appl., (2018).

[51] M. Schreiber, P. S. Peixoto, T. Haut, and B. Wingate, *Beyond spatial scalability limitations with a massively parallel method for linear oscillatory problems*, The International Journal of High Performance Computing Applications, (2017), p. 1094342016687625.

[52] J. C. Schulze, P. J. Schmid, and J. L. Sesterhenn, *Exponential time integration using Krylov subspaces*, International journal for numerical methods in fluids, 60 (2009), pp. 591–609.

[53] W. C. Skamarock, J. B. Klemp, M. G. Duda, L. D. Fowler, S.-H. Park, and T. D. Ringler, *A Multiscale Nonhydrostatic Atmospheric Model Using Centroidal Voronoi Tesselations and C-Grid Staggering*, Mon. Wea. Rev., 140 (2012), pp. 3090–3105.

[54] A. St-Cyr and S. J. Thomas, *Nonlinear operator integration factor splitting for the shallow water equations*, Applied Numerical Mathematics, 52 (2005), pp. 429–448.

[55] A. Staniforth and J. Ct, *Semi-Lagrangian Integration Schemes for Atmospheric Models - A Review*, Mon. Wea. Rev., 119 (1991), pp. 2206–2223.

[56] M. Tokman, *Efficient integration of large stiff systems of ODEs with exponential propagation iterative (EPI) methods*, Journal of Computational Physics, 213 (2006), pp. 748–776.

[57] G. K. Vallis, *Atmospheric and oceanic fluid dynamics*, Cambridge University Press, 2017.

[58] D. L. Williamson, *The evolution of dynamical cores for global atmospheric models*, J. Meteorol. Soc. Jpn., 85B (2007), pp. 241–269.

[59] D. L. Williamson, J. B. Drake, J. J. Hack, R. Jakob, and P. N. Swarztrauber, *A standard test set for numerical approximations to the shallow water equations in spherical geometry*, J. Comput. Phys., 102 (1992), pp. 211–224.

[60] D. Xiu and G. E. Karniadakis, *A Semi-Lagrangian High-Order Method for NavierStokes Equations*, Journal of Computational Physics, 172 (2001), pp. 658 – 684.